Epithelial Fli1 deficiency drives systemic autoimmunity and fibrosis: Possible roles in scleroderma

Takehiro Takahashi,[1] Yoshihide Asano,[1] Koji Sugawara,[2] Takashi Yamashita,[1] Kouki Nakamura,[1] Ryosuke Saigusa,[1] Yohei Ichimura,[1] Tetsuo Toyama,[1] Takashi Taniguchi,[1] Kaname Akamata,[1] Shinji Noda,[1] Ayumi Yoshizaki,[1] Daisuke Tsuruta,[2] Maria Trojanowska,[3] and Shinichi Sato[1]

[1]Department of Dermatology, University of Tokyo Graduate School of Medicine, Bunkyo-ku, Tokyo 113-8655, Japan
[2]Department of Dermatology, Osaka City University Graduate School of Medicine, Abeno-ku, Osaka 545-8585, Japan
[3]Arthritis Center, Rheumatology, Boston University School of Medicine, Boston, MA 02118

Systemic sclerosis (SSc), or scleroderma, is a multisystem autoimmune disorder characterized by vasculopathy and fibrosis in the skin and internal organs, most frequently in the esophagus and lungs. Hitherto, studies on SSc pathogenesis centered on immune cells, vascular cells, and fibroblasts. Although dysregulated keratinocytes in SSc have been recently reported, the contribution of epithelial cells to pathogenesis remains unexplored. In this study, we demonstrated the induction of SSc-like molecular phenotype in keratinocytes by gene silencing of transcription factor Friend leukemia virus integration 1 (Fli1), the deficiency of which is implicated in SSc pathogenesis. Keratin 14–expressing epithelial cell–specific *Fli1* knockout mice spontaneously developed dermal and esophageal fibrosis with epithelial activation. Furthermore, they developed remarkable autoimmunity with interstitial lung disease derived from thymic defects with down-regulation of autoimmune regulator (Aire). Importantly, Fli1 directly regulated Aire expression in epithelial cells. Collectively, epithelial Fli1 deficiency might be involved in the systemic autoimmunity and selective organ fibrosis in SSc. This study uncovers unidentified roles of dysregulated epithelial cells in SSc pathogenesis.

INTRODUCTION

Systemic sclerosis (SSc), or scleroderma, is a chronic connective tissue disease characterized by three cardinal features: autoimmunity/inflammation, vasculopathy, and fibrosis in the skin and various internal organs (Asano, 2010; Asano and Sato, 2015). Although SSc pathogenesis remains elusive, genetic studies have demonstrated that most of the susceptibility genes for SSc are HLA haplotypes and non-HLA genes related to immunity and inflammation, suggesting the central role of immune abnormalities in SSc development (Agarwal and Reveille, 2010). Indeed, during the early and sclerotic phases, the infiltration of activated T cells and macrophages and the degranulation of mast cells are observed in the affected skin, which correlate with the severity of skin thickening (Fleischmajer et al., 1977). With regard to $CD4^+$ T cells, the T helper type 1 cell (Th1 cell)/Th2 cell and Th17 cell/regulatory T cell (T reg cell) balances shift to Th2 and Th17 lineage dominance, respectively (O'Reilly et al., 2012). In particular, the increased expression of several Th2 cytokines, such as IL-6 and IL-13, contributes to fibroblast activation (Khan et al., 2012). In addition, despite the rarity of B cell infiltration in the skin, a cluster of B cell–related genes is strongly expressed in lesional and nonlesional skin of SSc patients (Whitfield et al., 2003). SSc B cells are constitutively activated, as represented by the increased expression of CD19, a critical positive response regulator (Sato et al., 2004), and produce various autoantibodies, including disease-specific antinuclear antibodies (ANAs) and other pathogenic antibodies against disease-related molecules (Sato et al., 2000; Hamaguchi, 2010). In interstitial lung disease (ILD) associated with SSc (SSc-ILD), activated B cells characteristically form aggregates in the lungs (Lafyatis et al., 2007). Supporting the critical role of B cells in SSc-ILD, rituximab, an anti-CD20 antibody, has proven efficacious in controlling ILD in a subset of patients (Lafyatis et al., 2009; Jordan et al., 2015). The initial immune activation and autoimmunity lead to the structural and functional abnormalities of vasculature and the constitutive activation of fibroblasts of SSc in various organs (Asano and Sato, 2015). However, the initial triggers of the dysregulated immune homeostasis and the origin of autoimmunity in this disease remain obscure (Harris and Rosen, 2003; Boin and Rosen, 2007; Joseph et al., 2014). Furthermore, although tissue fibrosis most commonly affects the skin, esophagus, and lungs in SSc (Gabrielli et al., 2009), a convincing ex-

Correspondence to Yoshihide Asano: yasano-tky@umin.ac.jp

Abbreviations used: Aire, autoimmune regulator; ANA, antinuclear antibody; ChIP, chromatin immunoprecipitation; CTGF, connective tissue growth factor; dcSSc, diffuse cutaneous SSc; EBS, Ets consensus binding site; EMT, epithelial–mesenchymal transition; EpCAM, epithelial cell adhesion molecule; Fli1, Friend leukemia virus integration 1; H&E, hematoxylin and eosin; HPF, high power field; ILD, interstitial lung disease; lcSSc, limited cutaneous SSc; mTEC, medullary TEC; NHK, normal human keratinocyte; qRT-PCR, quantitative RT-PCR; SCR, scrambled RNA; SSc, systemic sclerosis; TEC, thymic epithelial cell; TSA, tissue-specific self-antigen.

The Rockefeller University Press $30.00
J. Exp. Med. 2017 Vol. 214 No. 4 1129–1151
https://doi.org/10.1084/jem.20160247

planation for this distinct target organ specificity is currently lacking. Hence, these unresolved key questions in this disease remain to be addressed.

Reflecting the main disease manifestations, the majority of previous studies on SSc have centered on immune cells, vascular endothelial cells, and fibroblasts. However, more recent studies have demonstrated anomalous phenotypes of the skin epithelium, or keratinocytes, in SSc (Leask, 2009; Aden et al., 2010; Nikitorowicz-Buniak et al., 2014, 2015; Suwara et al., 2014; Assassi et al., 2015). For example, SSc keratinocytes persistently express wound-associated keratins keratin 6 (K6) and K16 not only in the sclerotic skin, but also in the nonlesional skin (Aden et al., 2010), suggesting that the altered epithelial phenotype manifests early in this disease. Besides, SSc keratinocytes stimulate fibroblasts in cell culture with excessively secreted IL-1α (Aden et al., 2010), which is a major alarmin released from the epithelial cells triggering an inflammatory response in fibroblasts (Suwara et al., 2014). Increased expression of the key profibrotic growth factor connective tissue growth factor (CTGF) is also evident in SSc epidermis (Leask, 2009; Nikitorowicz-Buniak et al., 2014). Additionally, epithelial–mesenchymal transition (EMT), a central mechanism in fibrosis development driven by TGF-β1 (Nieto et al., 2016), is enhanced in SSc epidermis with the increased expression of its cardinal regulator SNAI1 (Nakamura and Tokura, 2011; Wei et al., 2011; Nikitorowicz-Buniak et al., 2015). Of particular relevance is a recent study on global gene profiling of SSc lesional skin describing a correlation between specific keratin expression signatures and the presence of ILD (Assassi et al., 2015). Therefore, it seems that the epithelial phenotype is not merely related directly to dermal fibrosis but, more profoundly, associated with SSc development itself.

Numerous studies from our laboratory and others have demonstrated the critical role of Friend leukemia virus integration 1 (Fli1), a member of the Ets transcription factor family, in SSc pathogenesis. Fli1 is constitutively suppressed in dermal fibroblasts, dermal microvascular endothelial cells, and perivascular inflammatory cells not only in the lesional skin, but also in the nonlesional skin of SSc patients, at least in part, by an epigenetic mechanism (Kubo et al., 2003; Wang et al., 2006; Asano, 2015). Fli1 deficiency reproduces SSc-like phenotypes in dermal fibroblasts and dermal microvascular endothelial cells at molecular levels in vitro and in vivo (Asano et al., 2009; Noda et al., 2012, 2013; van Bon et al., 2014; Akamata et al., 2015a; Ichimura et al., 2015; Saigusa et al., 2015; Takahashi et al., 2015b; Romano et al., 2016). Consistently, bleomycin injection induces more prominent SSc-like phenotypes in *Fli1*$^{+/-}$ mice compared with wild-type mice (Taniguchi et al., 2015), whereas endothelial cell–specific *Fli1* knockout mice reproduce functional and structural vascular abnormalities characteristic of SSc vasculopathy (Asano et al., 2010a; Akamata et al., 2015b). Most importantly, double heterozygous mice for *Fli1* and Krüppel-like factor 5 (*Klf5*), another transcription factor epigenetically suppressed in SSc dermal fibroblasts, spontaneously develop three cardinal features of SSc, including autoimmunity/inflammation, vasculopathy, and tissue fibrosis of the skin and lungs, with the disease-specific pathological cascade (Noda et al., 2014). Thus, Fli1 deficiency is now considered as a key predisposing factor in SSc pathogenesis.

In the course of our study, we have consistently observed a substantial decrease of Fli1 expression also in keratinocytes. Collectively with the recent studies on SSc keratinocytes, this preliminary observation encouraged us to investigate the potential role of Fli1-deficient keratinocytes in SSc. Notably, our findings indicate that Fli1 deficiency in epithelial cells drives dermal and esophageal fibrosis as well as ILD through the induction of epithelial cell activation and immune self-intolerance caused by thymic defects, suggesting a critical role of epithelial Fli1 deficiency in the development of autoimmunity and selective organ fibrosis in SSc. Now, we believe that this might be a new clue to resolve the unaddressed key questions in this disease.

RESULTS

Fli1 down-regulation leads to the induction of SSc-like gene expression profiles in keratinocytes

We initially confirmed our unpublished observation that Fli1 expression is decreased in SSc keratinocytes. The immunostaining verified marked down-regulation of Fli1 in keratinocytes in addition to the previously reported deficiency in dermal fibroblasts and dermal microvascular endothelial cells in SSc patients (Fig. 1 A; Asano et al., 2010a). Because SSc is classified into two distinct subtypes, namely, diffuse cutaneous SSc (dcSSc) with skin sclerosis extending proximal to the elbow and limited cutaneous SSc (lcSSc) with skin sclerosis only distal to the elbow (LeRoy et al., 1988), the signal intensity was evaluated by a four-point grading scale in these subtypes. Of note, the decreased signal intensity in keratinocytes reached a statistical significance in dcSSc patients but not in lcSSc patients, compared with closely age- and sex-matched healthy controls (Fig. 1 B). In the epidermal sheets, consistently, *FLI1* mRNA was significantly down-regulated in dcSSc patients compared with healthy controls, whereas the increase in *K6*, *K16*, *IL1A*, *CTGF*, and *SNAI1* mRNAs was evident in dcSSc patients, some of which are known to be up-regulated in SSc epidermis (Fig. 1 C; Nikitorowicz-Buniak et al., 2014, 2015).

Next, we studied the impact of Fli1 deficiency on protein expression profiles of normal human keratinocytes (NHKs) in vitro. When transfected with *FLI1* siRNA, the expressions of several molecules associated with the altered phenotype of SSc keratinocytes, including keratins K6 and K16, as well as IL-1α, CTGF, and SNAI1 (Aden et al., 2010; Nikitorowicz-Buniak et al., 2014, 2015) were increased in NHKs (Fig. 1 D). However, Fli1 knockdown did not affect E-cadherin expression, whose down-regulation is another indicator of EMT as well as SNAI1 (Fig. 1 D). In line with these data, the increased expression of *SNAI1* mRNA but not *CDH1* mRNA was confirmed in NHKs transfected with

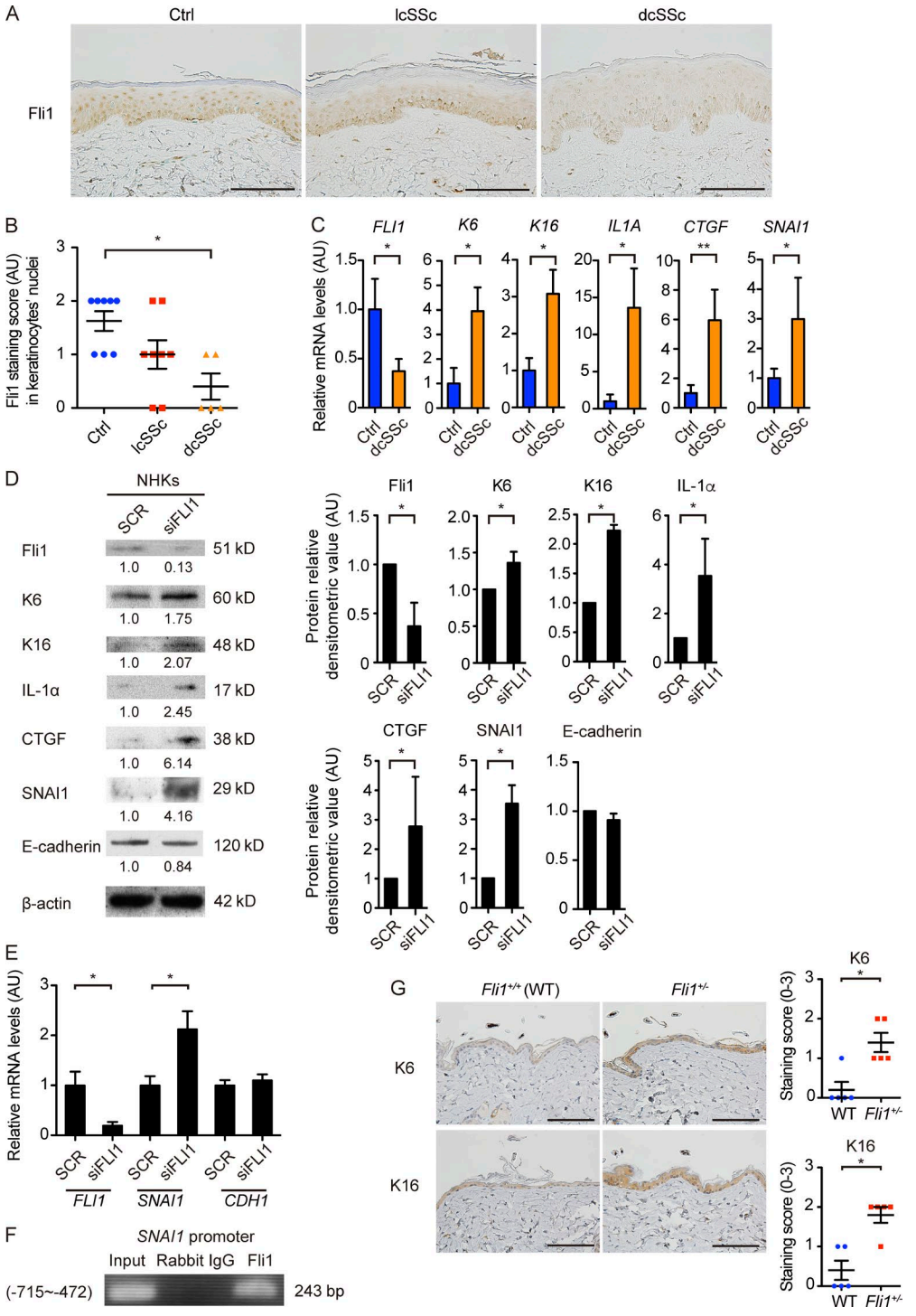

Figure 1. **Gene silencing of Fli1 leads to the induction of SSc-like protein and gene expression profiles in keratinocytes.** (A) Immunohistochemistry for Fli1 on the skin sections of healthy controls ($n = 8$), lcSSc patients with anticentromere antibody ($n = 8$), and dcSSc patients with anti–topoisomerase I antibody ($n = 5$). Representative images are shown. Bars, 100 µm. (B) The results of Fli1 staining intensity in A were semiquantitatively evaluated with a four-point grading scale. Kruskal-Wallis test followed by Dunn's posthoc test was used. (C) mRNA was isolated from skin epidermal sheets from healthy controls ($n = 4$) and dcSSc patients ($n = 6$), and gene expressions were analyzed by qRT-PCR. (D) Whole cell lysates from cultured NHKs treated with control nonsilencing SCR or *FLI1* siRNA (siFLI1) were subjected to immunoblotting. The values below each blot represent the relative levels of target molecules normalized by controls with densitometry. Representative images of the blots of four independent experiments are shown. (Right) The bar graphs summarize the relative values of the density from these four experiments. (E) The mRNA expression of *FLI1*, *SNAI1*, and *CDH1* in NHKs treated with SCR or siFLI1

FLI1 siRNA (Fig. 1 E), and Fli1 occupied the *SNAI1* promoter as shown by chromatin immunoprecipitation (ChIP; Fig. 1 F). Consistent with these in vitro observations, K6 and K16 were highly expressed in keratinocytes of $Fli1^{+/-}$ mice compared with those of wild-type ($Fli1^{+/+}$) mice in vivo (Fig. 1 G). Collectively, these results indicate the critical role of Fli1 deficiency in the induction of SSc-like properties in keratinocytes.

Conditional deletion of Fli1 in K14-expressing epithelial cells recapitulates the phenotype of SSc epidermis in vivo

To investigate the potential role of Fli1-deficient epithelial cells in SSc pathogenesis, we generated conditional *Fli1* knockout mice using the Cre-loxP system. We crossed $Fli1^{flox/flox}$ mice (Asano et al., 2010b) with mice expressing Cre recombinase under the control of the *K14* gene promoter (*K14Cre* mice), widely used to create keratinocyte-specific conditional knockout mice. Of note, Cre recombinase is also expressed in esophageal stratified squamous epithelia and medullary thymic epithelial cells (TECs; mTECs) of *K14Cre* mice (Qiu et al., 2011). $Fli1^{flox/flox}K14^{Cre/-}$ mice (*K14Cre;fl/fl* mice) and their littermate $Fli1^{flox/flox}$ mice (*fl/fl* mice) were used in this study.

K14Cre;fl/fl mice were born according to the normal Mendelian ratio and grew up without obvious abnormality, except that these mice were generally smaller in size than their littermate *fl/fl* mice (Fig. 2 A). The efficient down-regulation of Fli1 was confirmed by immunostaining in epidermal and follicular keratinocytes in *K14Cre;fl/fl* mice (Fig. 2 B). Concerning the epidermal phenotype, K6, K16, IL-1α, CTGF, and SNAI1 expressions in keratinocytes were significantly up-regulated in *K14Cre;fl/fl* mice compared with *fl/fl* mice (Fig. 2, C and D). Importantly, the expressions of IL-1α and CTGF were augmented also in dermal fibroblasts of *K14Cre;fl/fl* mice, as reported in SSc (Fig. 2 C; Kawaguchi et al., 2004; Noda et al., 2014). Furthermore, the analysis on gene expression profiles in epidermal sheets revealed increased mRNA expressions of the *K6*, *K16*, *Il1a*, *Ctgf*, and *Snai1* genes as well as significantly suppressed *Fli1* mRNA expression, mimicking the results of dcSSc skin epidermis (Fig. 2 E). These results indicate that epithelial Fli1 deficiency largely recapitulates the epidermal phenotype characteristic of dcSSc in vivo.

K14Cre;fl/fl mice spontaneously develop dermal fibrosis similar to that of SSc

We proceeded to analyze the skin as a whole including the dermis. Dermal fibrosis with a thickened dermis, more densely packed collagen bundles, and enhanced signal intensity of Masson-Trichrome staining was observed in *K14Cre;fl/fl* mice, becoming evident at the age of 3 mo (Fig. 3, A and B). Fibrosis was homogenous throughout the dermis without predominance of the subepithelial upper dermis (Fig. 3 A). As well, total collagen content was elevated in the skin of *K14Cre;fl/fl* mice, reaching a statistical significance at the age of 3 mo (Fig. 3 C). Moreover, *Col1a1* and *Col1a2* mRNA expressions and the number of myofibroblasts were also increased in the skin of *K14Cre;fl/fl* mice at the age of 3 mo (Fig. 3, D and E). However, unlike human SSc and its several mouse models (Marangoni et al., 2015), there was no evident subcutaneous adipose tissue atrophy in *K14Cre;fl/fl* mice (Fig. 3 F). Further analyses using electron microscopy delineated mildly increased thickness and diameter variability in the collagen fibrils in *K14Cre;fl/fl* mice (Fig. 3 G), consistent with the impairment of collagen fibrillogenesis as represented by the up-regulation of fibrillogenesis-related molecules such as ADAMTS2 (a disintegrin and metalloproteinase with thrombospondin motif 2) and lumican (Fig. 3 H). These alterations related to collage fibrillogenesis are reminiscent of the previously reported changes in SSc dermis (Perlish et al., 1988; Noda et al., 2014).

With respect to inflammatory components, the perivascular infiltration of T cells, macrophages, and mast cells was augmented throughout the whole dermis in *K14Cre;fl/fl* mice by the age of 2 mo, without evidence of interface dermatitis (Fig. 3, I and J). The analysis of the expression profiles of several key profibrotic/proinflammatory cytokines, chemokines, and growth factors disclosed the heightened expression of *Il1b*, *Il6*, *Il13*, *Il17a*, *Ccl2*, *Tgfb1*, and *Ctgf* mRNAs in the skin of *K14Cre;fl/fl* mice (Fig. 3 K), also simulating the expression profiles in SSc lesional skin. Collectively, these results indicate that epithelial Fli1 deficiency is sufficient to induce a pathological dermal fibrosis similar to that of SSc at histological, morphological, and molecular levels in mice.

K14Cre;fl/fl mice recapitulate esophageal involvement of SSc

We further examined the esophagus, the second most frequently affected organ in SSc, because it has stratified squamous epithelia expressing K14 (Gabrielli et al., 2009). Augmented collagen deposition as represented by enhanced signal intensity of Masson-Trichrome staining was evident in the subepithelial lamina propria in the lower esophagus of aged *K14Cre;fl/fl* mice, and the increase in the thickness of this layer, which was reminiscent of esophageal and gas-

was evaluated. Relative expression levels from four independent experiments were normalized to the expression levels treated with SCR. (F) ChIP assay in NHKs was performed with anti-Fli1 antibody and the primers specific for the designated area of the *SNAI1* gene promoter. (G) The back skin taken from $Fli1^{+/-}$ mice and their littermate wild-type ($Fli1^{+/+}$) mice were immunohistochemically stained for K6 and K16. $n = 5$ for each group. (Left) Representative images of immunohistochemistry are shown. Bars, 100 µm. (Right) The graphs show the results of semiquantitative scoring of the staining intensity. Data are shown as mean ± SEM. *, $P < 0.05$; **, $P < 0.01$; by two-tailed Mann-Whitney *U* test, unless otherwise indicated. The results are from representative experiments that have been repeated twice independently or are otherwise indicated. AU, arbitrary units; Ctrl, control.

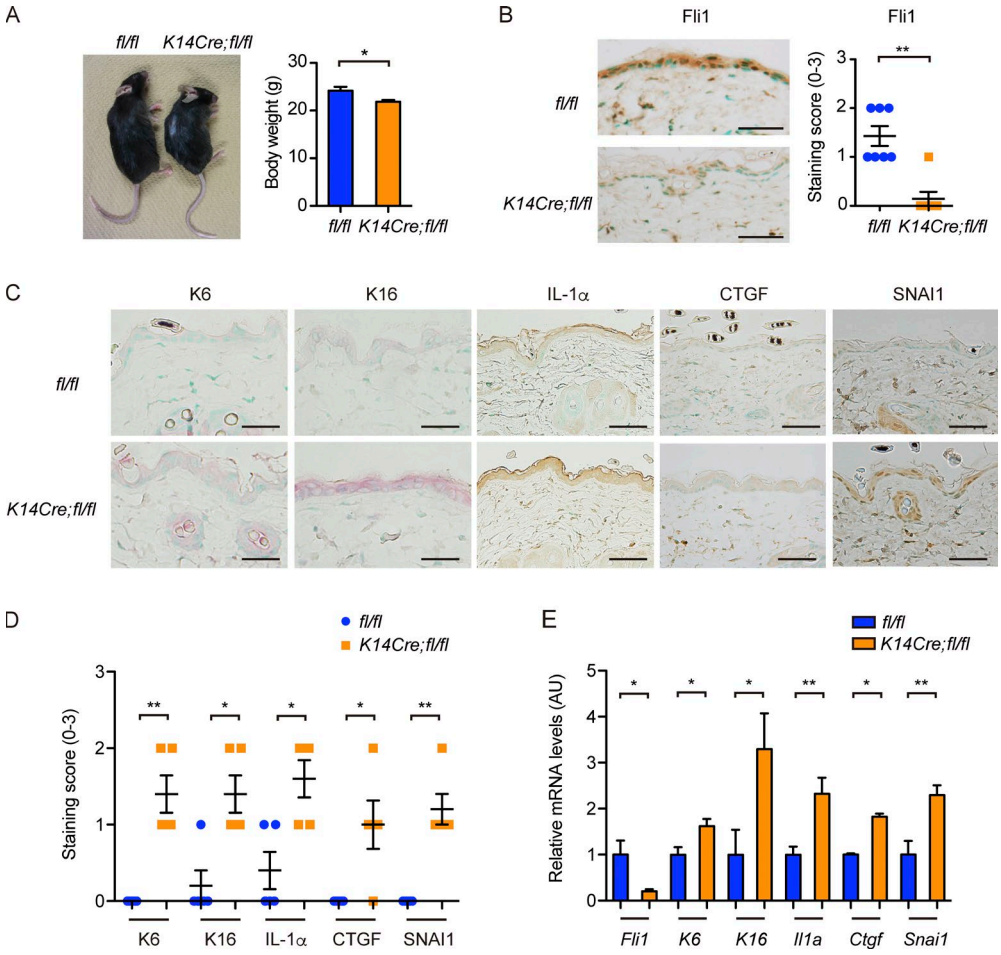

Figure 2. ***K14Cre;fl/fl* mice exhibit SSc-like epidermal phenotypes.** (A, left) A representative image of mice at ∼4 mo of age. (Right) The comparison of body weight between two strains of mice. $n = 7$ per genotype. (B, left) Immunohistochemistry for Fli1 in the back skin of mice. Bars, 50 µm. (Right) The graph summarizes the result of semiquantitative scoring of the staining intensity. $n = 7$ per genotype. (C) Immunohistochemistry for K6, K16, IL-1α, CTGF, and SNAI1 in the back skin of mice. $n = 5$ per genotype. Bars, 50 µm. (D) The results of staining intensity in the epidermis as shown in C were evaluated with semiquantitative scoring. $n = 5$ per genotype. (E) mRNA expressions of these key molecules were determined by qRT-PCR in the epidermal sheets prepared from the back skin of mice. $n = 5$ per genotype. Data are shown as mean ± SEM. *, $P < 0.05$; **, $P < 0.01$; by two-tailed Mann-Whitney *U* test. The results are from representative experiments that have been repeated twice in different pairs of mice with similar results. Representative images of immunohistochemistry are shown. AU, arbitrary units.

tric wall alteration in SSc (Manetti et al., 2007; Taroni et al., 2015), became overt by the age of 3 mo (Fig. 4, A and B). The increased lamina propria thickness was also observed in the upper esophagus above the esophageal hiatus in *K14Cre;fl/fl* mice (Fig. 4 C). In contrast, the thickness of the circular muscle layer tended to be decreased in the lower esophagus of *K14Cre;fl/fl* mice with augmented collagen deposition between the muscular fibers (Fig. 4, A and D), resembling SSc esophagus (Roberts et al., 2006). Increased collagen deposition in the esophagus of *K14Cre;fl/fl* mice was even more supported by the results of hydroxyproline assay (Fig. 4 E). Moreover, gene expressions of fibrosis-related molecules, cytokines, and growth factors, such as *Col1a1*, *Col1a2*, *Il1b*, *Il6*, *Il8*, and *Tgfb1*, were up-regulated in the lower esophagus of *K14Cre;fl/fl* mice (Fig. 4 F). The augmented expression of IL-1β was also immunohistochemically confirmed in the esophageal epithelial cells of *K14Cre;fl/fl* mice (Fig. 4 G), further supporting the activation of esophageal epithelial cells. Considering the up-regulation of *IL1B*, *IL6*, and *IL8* mRNAs in SSc esophagus (Rieder et al., 2010; Taroni et al., 2015), these results suggest that *K14Cre;fl/fl* mice recapitulate the histological and molecular features of SSc esophageal disease.

K14Cre;fl/fl mice spontaneously develop ILD

Further examination of histological changes in various internal organs revealed enhanced mononuclear cell infiltration into the lung interstitium (Fig. 4 H), whereas other internal organs, such as the heart, liver, kidney, stomach, small intestine, and large intestine, did not show evident fibrosis or inflammation (not depicted). The inflammatory cell infiltration in

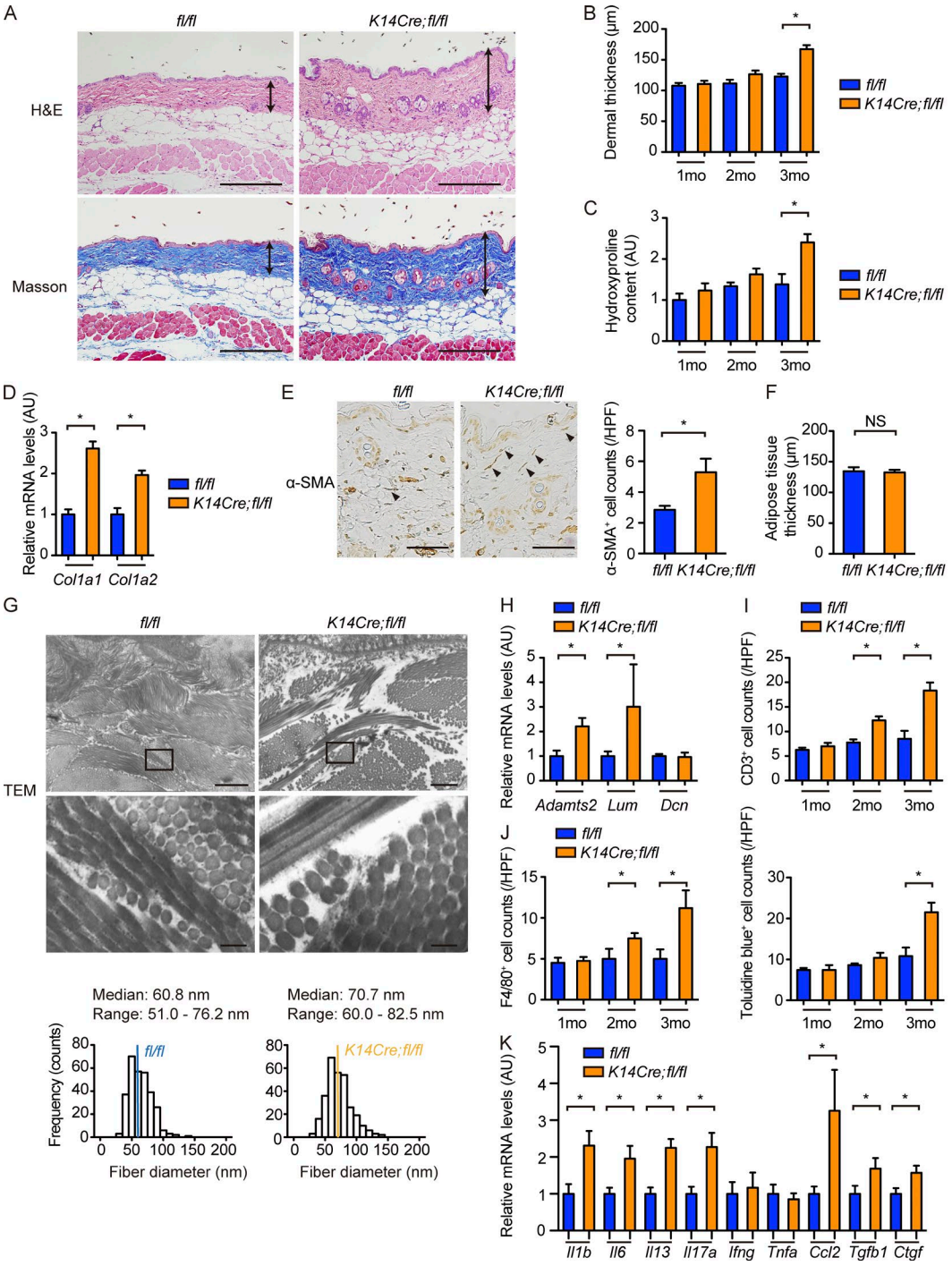

Figure 3. ***K14Cre;fl/fl* mice spontaneously develop SSc-like dermal fibrosis.** (A) H&E and Masson-Trichrome staining of the back skin of 3-mo-old mice. Double-headed arrows represent dermal thickness. Bars, 200 µm. (B) The dermal thickness was evaluated at the ages of 1, 2, and 3 mo in each group of mice. (C) Hydroxyproline contents of the back skin were compared between two strains of mice at the ages of 1, 2, and 3 mo. The values are normalized to the value of 1-mo-old *fl/fl* mice. (D) mRNA expressions of the *Col1a1* and *Col1a2* genes were measured by qRT-PCR in the back skin of 3-mo-old mice. (E) Skin sections from 3-mo-old mice were stained for α-SMA. (Left) Representative images of the staining, with arrowheads pointing to α-SMA–positive myofibroblasts. Bars, 50 µm. (Right) The bar graph shows the number of α-SMA–positive myofibroblasts per HPF. (F) Adipose tissue thickness in each group of mice was evaluated at the age of 3 mo. (G) Transverse and longitudinal sections of collagen fiber alignment in the superficial dermis were examined by transmission electron microscopy (TEM). (Middle) Higher magnification images of the regions indicated by squares in the top panels. Bars: (top) 1 µm; (middle) 100 nm. (Bottom) Median, range, and frequency distribution profiles obtained by manually measuring the smallest diameter of 300 collagen fibrils are summarized. Colored bars in the histogram indicate the median of each group. *n* = 3 mice per genotype. (H) mRNA expressions of genes related to

the lungs was enhanced to the slightly noticeable level already at the age of 1 mo and became more prominent along with aging especially in the peribronchial areas in *K14Cre;fl/fl* mice (Fig. 4 H). By the age of 3 mo, several mice with severe disease developed peribronchial lymphocyte aggregates or lymphoid structures composed of T and B cells, resembling inducible bronchus-associated lymphoid tissues (Fig. 4, H and I), which occur in the settings of chronic inflammation, including ILD, in human autoimmune diseases (Rangel-Moreno et al., 2006). Total collagen content was mildly increased, and interstitial fibrosis was particularly salient in the peribronchial interstitium as shown by Masson-Trichrome staining (Fig. 4 J). Furthermore, expression of IL-1β, IL-6, IL-13, IL-17A, and CCL2, known to play important roles in the development of ILD (Wilson and Wynn, 2009), was up-regulated at the mRNA level (Fig. 4 K), suggesting that Th2/Th17 cell–skewed immune polarization is involved in ILD in *K14Cre;fl/fl* mice. In aggregate, the emergence of dermal and esophageal fibrosis together with ILD in *K14Cre;fl/fl* mice indicated striking similarities of the fibrotic and autoimmune phenotypes between these mice and human SSc.

K14Cre;fl/fl mice exhibit prominent Th2/Th17 cell polarization and abnormal B cell activation together with the emergence of autoantibodies

The immune changes in the affected organs of *K14Cre;fl/fl* mice suggested systemic immune activation polarized toward the Th2/Th17 axis. Further analyses of mutant mice revealed splenomegaly and lymphadenopathy together with the increased number of splenocytes (Fig. 5, A and B). Intracellular cytokine staining of $CD4^+$ T cells isolated from lymph nodes showed enhanced proportion of IL-4/IL-17A–positive cells in 3-mo-old *K14Cre;fl/fl* mice, supporting the presence of Th2/Th17 cell–skewed immune polarization (Fig. 5 C). Under the same condition, CD19 expression was augmented ∼12% on splenic B cells ($B220^+CD19^+$ cells; Fig. 5 D), possibly reflecting their abnormal activation because an ∼20% increase in CD19 expression was observed in activated B cells from SSc patients and human CD19 transgenic mice producing excessive amount of autoantibodies (Saito et al., 2002). Consistently, serum levels of total IgG and IgM were elevated in 3-mo-old *K14Cre;fl/fl* mice, which became more evident in older mice (Fig. 5 E). Serum concentration of IL-6, a key cytokine in SSc pathogenesis (O'Reilly et al., 2013), was significantly higher in *K14Cre;fl/fl* mice as early as 2 mo of age, and its elevation got more remarkable along with aging (Fig. 5 F). B cell activation in *K14Cre;fl/fl* mice was further supported by the increased IL-6 concentration in the culture supernatant of isolated B cells (Fig. 5 G). Moreover, ANA was detected in *K14Cre;fl/fl* mice as early as 2 mo of age (two out of eight mice in 2-mo-old mice, six out of eight mice in 3-mo-old mice, and seven out of eight mice in 8-mo-old mice), whereas not at all in control *fl/fl* mice ($n = 8$ at each time point; Fig. 5 H). Elevated ANA titers in *K14Cre;fl/fl* mice were also confirmed by ELISA (Fig. 5 H). To more strictly confirm the presence of systemic autoimmune response, autoantibodies against self-proteins were assessed by immunoblotting using homogenates from the lungs of $Rag1^{-/-}$ mice, which lack their intrinsic immunoglobulins. The blotting of electrophoresed $Rag1^{-/-}$ mice lung homogenates with sera from *K14Cre;fl/fl* mice disclosed the presence of autoantibodies against certain lung proteins in these mice (Fig. 5 I). Collectively, these findings suggest the emergence of robust systemic autoimmunity in *K14Cre;fl/fl* mice, characterized by the prominent Th2/Th17 cell polarization and abnormal B cell activation with autoantibody production.

mTECs robustly express Fli1

The autoimmune phenotype in *K14Cre;fl/fl* mice prompted us to focus on the thymus, the central organ for immune self-tolerance consisting of thymocytes and two kinds of TECs, cortical TECs and mTECs. Because mTECs abundantly express K5 and K14, Cre recombinase under the control of *K5* or *K14* promoter was used to create mTEC-specific conditional knockout mice (Sano et al., 2001; Sukseree et al., 2012). Various tissue-specific self-antigens (TSAs) are expressed by mTECs under the control of master regulators, including autoimmune regulator (Aire), resulting in the elimination of autoreactive T cells by apoptosis and the development of T reg cells in the thymus (Anderson et al., 2002; Mathis and Benoist, 2009). Importantly, the decrease in Aire expression suppresses the expression of TSAs dose dependently, allowing escape of autoreactive T cells from negative selection (Liston et al., 2004; Kont et al., 2008), and affects the development and differentiation of mTECs (Matsumoto, 2011). Given that Fli1 is abundantly expressed in the thymus (Mélet et al., 1996; Qiu et al., 2011), we hypothesized that immune activation and autoimmunity of *K14Cre;fl/fl* mice might be caused by the thymic abnormalities. To address this issue, we analyzed Fli1 expression in the thymuses of wild-type (C57BL/6) mice. Indeed, the immunostaining of Fli1 in the thymuses of wild-type mice illustrated scattered strong positivity in the nuclei of the cells almost exclusively confined to the thymic medulla (Fig. 6 A). Supportively, double immunofluorescence

collagen fibrillogenesis were determined by qRT-PCR in the back skin of 3-mo-old mice. (I and J) Inflammatory cell infiltrations in the back skin at the ages of 1, 2, and 3 mo were assessed per HPF. Immunostaining for CD3 (I) and F4/80 (J, left) and toluidine blue staining (J, right) were performed to count T cells, macrophages, and mast cells, respectively. (K) mRNA levels of key cytokines, chemokines, and growth factors were assessed by qRT-PCR in the back skin of 3-mo-old mice. Data are shown as mean ± SEM. *, $P < 0.05$ by two-tailed Mann-Whitney *U* test. $n = 4 – 5$ mice per genotype, unless otherwise indicated. The results are from representative experiments that have been repeated three times in different pairs of mice with similar results. Representative images of H&E, Masson-Trichrome, and α-SMA staining and transmission electron microscopy are shown. AU, arbitrary units.

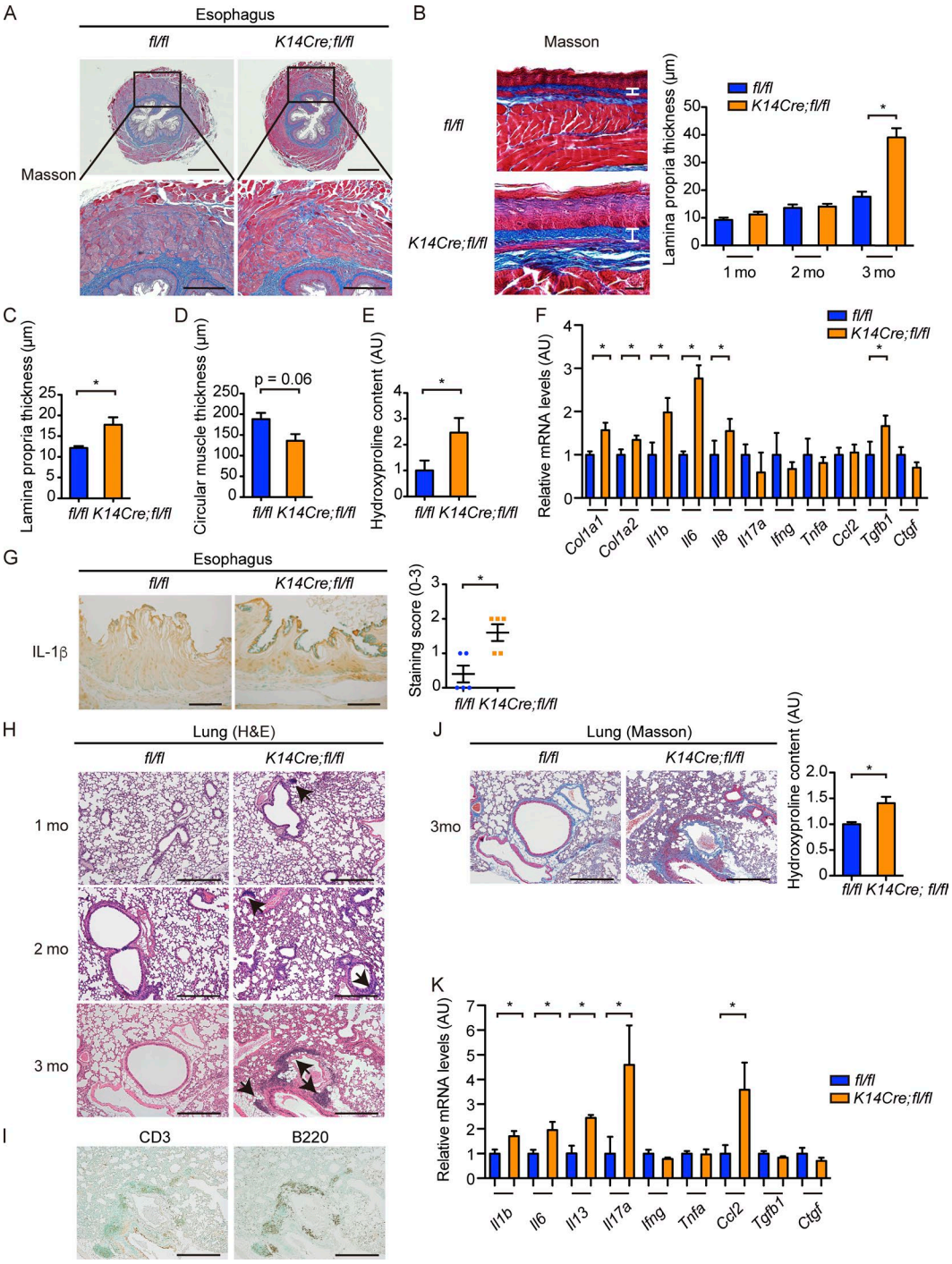

Figure 4. ***K14Cre;fl/fl* mice develop esophageal fibrosis and ILD.** (A) Masson-Trichrome staining of the lower esophagus of 3-mo-old *fl/fl* and *K14Cre;fl/fl* mice. (Bottom) Higher magnification images of the regions indicated by squares in the top panels. Bars: (top) 500 µm; (bottom) 200 µm. (B) The lower esophagi were cut along the longitudinal direction, spread on sheets, fixed in formalin, and embedded in the paraffin. Masson-Trichrome staining was performed, and the thickness of the lamina propria was evaluated at the ages of 1, 2, and 3 mo. Vertical bars represent lamina propria thickness. Bars, 50 µm. (C) The thickness of lamina propria at upper (thoracic) esophagus was evaluated at the age of 3 mo. (D) The thickness of the circular muscle layer was evaluated in the sections of 3-mo-old mice. (E) Hydroxyproline contents of the lower esophagus were compared between these two strains of mice at the age of 3 mo. (F) mRNA levels of type I collagen, cytokines, chemokines, and growth factors in the lower esophagi of 3-mo-old mice were assessed. (G) The lower esophagus sections from 3-mo-old mice were immunohistochemically stained for IL-1β. Bars, 50 µm. (Right) The graph shows the result of semiquantitative scoring of the staining intensity. (H) H&E staining of the lungs from 1-, 2-, and 3-mo-old *fl/fl* and *K14Cre;fl/fl* mice. Arrows indicate the peribronchial lymphocyte aggregates. Bars, 200 µm. (I) Infiltrating inflammatory cells were immunohistochemically stained for CD3 and B220 in the lungs

revealed the weak signal intensity of Fli1 in thymocytes and strong signal intensity of Fli1 in the medullary stromal cells expressing Aire, indicating that mTECs abundantly express Fli1 (Fig. 6 B). Therefore, we hypothesized that *K14Cre;fl/fl* mice develop autoimmunity because of a Fli1 deficiency–dependent defect of the thymus, or especially of the mTECs, and proceeded to further investigations of the thymus.

Thymuses of *K14Cre;fl/fl* mice exhibit prominent atrophy with decreased expression of Aire

In line with our hypothesis, we found salient atrophy of thymuses with the significantly decreased number of thymocytes in *K14Cre;fl/fl* mice (Fig. 6, C and D). Hematoxylin and eosin (H&E) staining showed the reduced size of bright areas corresponding to thymic medulla and total medullary area and area per islet were significantly decreased (Fig. 6 E). Correspondingly, flow cytometric analyses of the thymic stromal cells revealed a significantly smaller number of mTECs (defined as $CD45^-$epithelial cell adhesion molecule $[EpCAM]^+Ly51^-$ cells) in *K14Cre;fl/fl* mice (Fig. 6 F). In immunostaining, both Fli1-positive cells and Aire-positive cells were notably decreased with a strong correlation in the thymic medulla of *K14Cre;fl/fl* mice (Fig. 6, G and H). Consistent with these findings, the analyses of mRNA expression in sorted mTECs demonstrated significantly suppressed *Fli1* and *Aire* gene expressions in *K14Cre;fl/fl* mice (Fig. 6 I). Also observed was the down-regulation of Aire-dependent as well as Aire-independent genes, such as *Ins2*, *Chrna1*, *Sp1*, *Col2a1*, and *Crp*, suggesting the defective presentation of self-antigens regulated by Aire and other transcription factors in their thymuses (Fig. 6 I). Because the presentation of self-antigens in mTECs plays an essential part in T reg cell development (Mathis and Benoist, 2009), we also assessed T reg cells in the thymuses. As expected, the proportion and number of thymic T reg cells (defined as $CD3^+CD4^+Foxp3^+$ cells) were significantly decreased in *K14Cre;fl/fl* mice (Fig. 6 J). Collectively, these results indicate that the thymuses of *K14Cre;fl/fl* mice exhibit an abnormality in mTEC development, including the suppressed expression of self-antigens by loss of Aire, and possibly other transcription factors, contributing to the development of the deletion-escaped autoreactive T cells underlying autoimmunity.

Development of ILD, but not dermal and esophageal fibrosis, in *K14Cre;fl/fl* mice is dependent on their autoreactive T cells

To verify whether deletion-escaped autoreactive T cells are responsible for autoimmunity in *K14Cre;fl/fl* mice, we transferred isolated T cells into *Rag1*$^{-/-}$ mice lacking intrinsic mature lymphocytes. As expected, transfer of $NK1.1^-CD3^+$ T cells isolated from *K14Cre;fl/fl* mice to *Rag1*$^{-/-}$ mice reproduced the prominent interstitial inflammatory cell infiltration, mainly composed of $CD3^+$ T cells, in the lungs with increased collagen deposition in the interstitium, whereas transfer from the littermate *fl/fl* mice did not (Fig. 7, A and B). These changes were seen as early as 2 mo after transfer and strikingly aggravated at 6 mo after transfer (Fig. 7 A). The analysis of various internal organs of recipient *Rag1*$^{-/-}$ mice at 6 mo after transfer demonstrated that such a prominent inflammatory phenotype was almost exclusive to the lungs, except some mice exhibiting moderately increased inflammatory cell infiltration in several organs, including the skin, liver, kidney, and esophagus (Fig. 7 C). Importantly, fibrosis was totally absent in the skin and esophagus even at 6 mo after transfer, confirmed with histological observation and measurements of collagen contents (not depicted). These results indicated that ILD development in *K14Cre;fl/fl* mice is primarily caused by autoreactive T cells, whereas dermal and esophageal fibrosis could not be caused by these cells alone.

To further analyze whether dermal and esophageal fibrosis is driven by their epithelia and/or systemic autoimmunity, we generated *Rag1*$^{-/-}$*;K14Cre;fl/fl* mice by crossing *Rag1*$^{-/-}$ mice and *K14Cre;fl/fl* mice. These mice lack mature lymphocytes, whereas the epithelial phenotype in the skin and esophagus is considered to be identical to that of *K14Cre;fl/fl* mice. We analyzed *Rag1*$^{-/-}$*;K14Cre;fl/fl* mice at the age of 3 mo, with their littermate *Rag1*$^{-/-}$*;fl/fl* mice as controls. Of note, the skin and esophagus of *Rag1*$^{-/-}$*;K14Cre; fl/fl* mice showed a significant increase in the thickness of dermis and lamina propria, respectively, compared with *Rag1*$^{-/-}$*;fl/fl* mice (Fig. 7, D–G). In accordance with the observation in *K14Cre;fl/fl* mice, inflammatory cell infiltration was enhanced in the skin of *Rag1*$^{-/-}$*;K14Cre;fl/fl* mice (Fig. 7 D), whereas ILD was totally absent (not depicted). In addition, collagen content in the skin and esophagus of *Rag1*$^{-/-}$*;K14Cre;fl/fl* mice was significantly increased compared with controls, although the ratio of increase was smaller than that between *K14Cre;fl/fl* mice and *fl/fl* mice (Fig. 7, E and G).

Next, we conducted splenocyte transfer from *fl/fl* mice to *Rag1*$^{-/-}$*;K14Cre;fl/fl* mice to analyze whether T cell–mediated autoimmunity in *K14Cre;fl/fl* mice is truly derived from the thymic abnormalities or, alternatively, from the systemic skin abnormality. If the autoimmunity is derived from the skin, the autoimmune phenotype should be reproduced in the recipient *Rag1*$^{-/-}$*;K14Cre;fl/fl* mice by the transferred lymphocytes, which are not originally autoreactive.

of 3-mo-old *K14Cre;fl/fl* mice. Bars, 200 µm. (J, left) The Masson-Trichrome staining of the lungs from 3-mo-old *fl/fl* and *K14Cre;fl/fl* mice. Bars, 200 µm. (Right) Collagen contents of the total left lung from these mice were measured by hydroxyproline assay. (K) mRNA levels of cytokines, chemokines, and growth factors in the lung of 3-mo-old mice were assessed by qRT-PCR. Data are shown as mean ± SEM. *, $P < 0.05$ by two-tailed Mann-Whitney *U* test. $n = 4–5$ mice per each genotype in all experiments. The results are from representative experiments that have been repeated three times in different pairs of mice with similar results. Representative images of H&E and Masson-Trichrome staining and immunohistochemistry are shown. AU, arbitrary units.

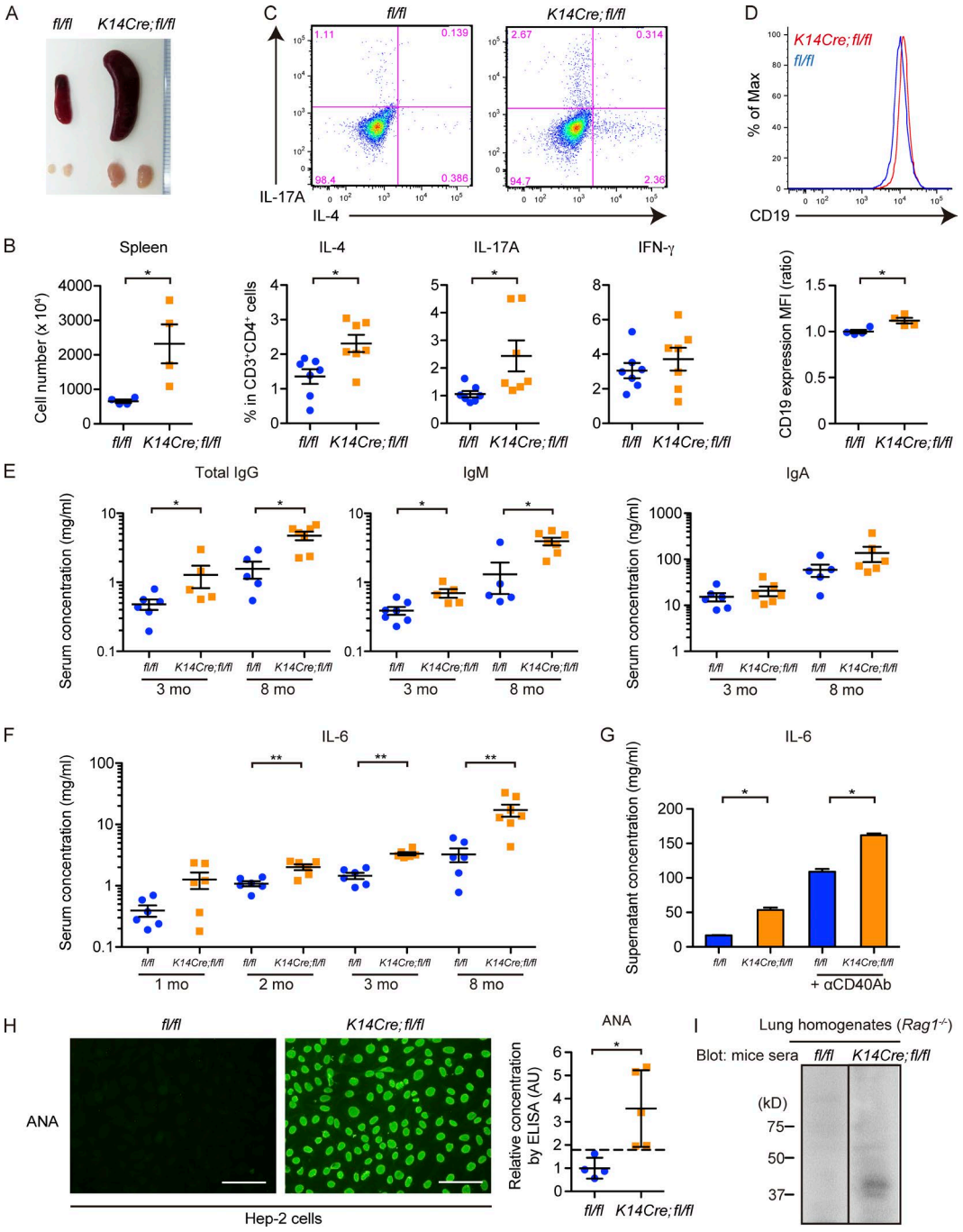

Figure 5. ***K14Cre;fl/fl* mice exhibit prominent autoimmunity with Th2/Th17 cell polarization and abnormal B cell activation leading to autoantibody production.** (A) A representative image of the gross appearance of spleens and inguinal lymph nodes from 3-mo-old *fl/fl* and *K14Cre;fl/fl* mice. (B) The number of splenocytes in 3-mo-old *fl/fl* and *K14Cre;fl/fl* mice was counted. $n = 4$ per each group. (C) Lymphocytes isolated from inguinal lymph nodes were stained for CD3 and CD4 and intracellularly stained for IL-4, IL-17A, and IFN-γ. (Top) Representative two-dimensional plots for IL-4 and IL-17A in $CD3^+CD4^+$ cells. (Bottom) The percentages of cells positive for IL-4, IL-17A, and IFN-γ are summarized. $n = 7$ mice per each group. (D) Splenocytes from 3-mo-old *fl/fl* and *K14Cre;fl/fl* mice were stained for B220 and CD19. $B220^+CD19^+$ cells were analyzed for CD19 expression. A representative histogram of mean fluorescence intensity (MFI; top) and the comparison of mean fluorescence intensities (bottom) are shown. $n = 4$ mice per genotype. (E) Sera from 3- and 8-mo-old mice were analyzed for the concentrations of total IgG, IgM, and IgA. $n = 5–7$ mice per genotype. Note that the results are shown with log scale. (F) Sera from 1-, 2-, 3-, and 8-mo-old mice were analyzed for the concentration of IL-6. $n = 6–7$ mice per genotype. (G) B cells were isolated from splenocytes of 3-mo-old mice and cultured for 48 h, either unstimulated or stimulated with anti-CD40 antibody (αCD40Ab). The culture supernatants were subject to the measurement of IL-6 concentration. $n = 4$ mice per each group. (H) The presence of ANA in the sera was assessed by indirect immunofluores-

We transferred 10^7 splenocytes from 3-mo-old *fl/fl* mice to 1-mo-old *Rag1*$^{-/-}$*;K14Cre;fl/fl* mice, sacrificed them 3 mo later, and analyzed the presence of serum ANA and ILD in the recipient mice, as these traits seem to be the hallmarks of the autoimmune phenotypes of *K14Cre;fl/fl* mice. The results showed negativity of ANA and ILD in all recipient *Rag1*$^{-/-}$*;K14Cre;fl/fl* mice (10 out of 10; not depicted). Collectively, these results suggest that tissue fibrosis in the skin and esophagus of *K14Cre;fl/fl* mice is principally driven by their epithelia, whereas the T cell–mediated autoimmunity leading to ILD depends on the thymic abnormality.

Fli1 serves as a potent transcriptional activator of the *AIRE* gene in epithelial cells

The thymic defects, including its atrophy and suppressed expression of Aire in *K14Cre;fl/fl*, mice prompted us to investigate whether Fli1 directly regulates Aire expression. Indeed, several Ets transcription factors, such as Ets1, Ets2, and ESE-1, have positive effects on *AIRE* transcription (Murumägi et al., 2006). Because of the difficulties in isolating and culturing mTECs, we used NHKs because Aire is also expressed in keratinocytes (Kumar et al., 2011). The analysis with the luciferase promoter construct revealed a markedly enhanced activity of the *AIRE* promoter in response to Fli1 overexpression (Fig. 8 A). ChIP assay displayed the binding of Fli1 to the *AIRE* promoter at −403/−235 bp upstream of the transcription start site (Fig. 8 B). This region contains three putative Ets consensus binding sites (EBS; GGAA/TTCC; Fig. 8 C). We mutated these EBSs (EBS-A/-B/-C) individually and assessed luciferase activity. The results showed particular importance of EBS-A (Fig. 8 C). Furthermore, the oligonucleotide pull-down assay verified the sequence-specific binding of Fli1 to EBS-A (Fig. 8 D). Thus, Fli1 serves as a potent transcriptional activator of the *AIRE* gene in epithelial cells.

Aire expression is decreased in SSc keratinocytes

Finally, we investigated the expression of Aire in SSc patients. Because of the limited availability of human thymus samples, we used human skin samples instead because Aire has been reported to be expressed in human keratinocytes in cell culture (Clark et al., 2005). The immunohistochemical analysis with the skin samples showed the expression of Aire abundantly in the nuclei of normal keratinocytes but moderately or weakly in the nuclei of SSc keratinocytes (Fig. 9 A). Notably, the expression was uniformly attenuated in almost all of the keratinocytes in dcSSc patients with anti–topoisomerase I antibody, which typically exhibit systemic autoimmunity and chronic inflammation resulting in multiple organ fibrosis, most frequent in the lungs and esophagus (Gabrielli et al., 2009). However, in lcSSc patients with anticentromere antibody, who manifest relatively milder or little fibrotic involvement of internal organs, the decrease in Aire expression was moderate to none, which was variable in individual keratinocytes. When evaluated by a four-point grading scale, the signal intensity was significantly decreased in dcSSc patients but not in lcSSc patients, compared with healthy controls (Fig. 9 B). Importantly, the staining intensity of Aire and Fli1 in the nuclei of keratinocytes revealed a significant positive correlation in the specimens from dcSSc patients and age- and sex-matched healthy controls in which both of these two molecules were analyzed together (Fig. 9 C). Consistent with these data, *AIRE* mRNA expression was significantly suppressed in SSc lesional skin compared with healthy control skin (Fig. 9 D) and positively correlated with *FLI1* mRNA expression (Fig. 9 E). Additionally, we failed to detect the correlation of Aire expression with inflammatory cytokines IL-6 and TNFα at the mRNA level, indicating the negative causality of inflammation in *AIRE* down-regulation (not depicted). We also performed Aire staining in the skin of mice, as well as in the thymuses of wild-type mice as positive controls, to examine whether relevant findings were confirmed in mice. The result showed negativity of Aire protein expression in keratinocytes or other cells in the skin of both groups of mice (not depicted). This result was in line with a previous study that demonstrated very low Aire expression in normal mice skin, whereas its expression is to some extent induced in certain situations such as skin tumors (Hobbs et al., 2015). Collectively, although the significance of Aire expression in human skin remains to be resolved, these findings seem to support the close relationship between Aire and Fli1 in humans.

DISCUSSION

In the field of SSc research, few previous studies have addressed the following simple question: why is SSc an autoimmune disease? Our present study might give a possible answer to this fundamental question: it is the epithelial Fli1 deficiency that is implicated in the development of immune activation toward self through defective thymic epithelial development together with down-regulation of the *AIRE* gene. Additionally, our study might provide a clue to another basic question on the characteristic organ specificity in this disease: why are the skin and esophagus the two most frequent targets of fibrosis in SSc? The answer might be the epithelial Fli1 deficiency that leads to the altered epithelial phenotype

cence with Hep-2 cells. (Left) The photographs show representative immunofluorescence images with sera from 2-mo-old mice. *n* = 8 mice per genotype. Bars, 100 µm. (Right) Titers of ANA in the sera were assessed with a specific ELISA. The dashed line indicates the mean + 2 SD value of *fl/fl* mice. *n* = 4–5 mice per genotype. (I) Immunoblotting of lung tissue lysates from *Rag1*$^{-/-}$ mice with sera from *fl/fl* and *K14Cre;fl/fl* mice. *n* = 3 mice sera per group. For photographs, immunofluorescence, and immunoblotting, representative results are shown. Data are shown as mean ± SEM. *, P < 0.05; **, P < 0.01; by two-tailed Mann-Whitney *U* test. The results are from representative experiments that have been repeated three times in different pairs of mice. AU, arbitrary units; MFI, mean fluorescence intensity.

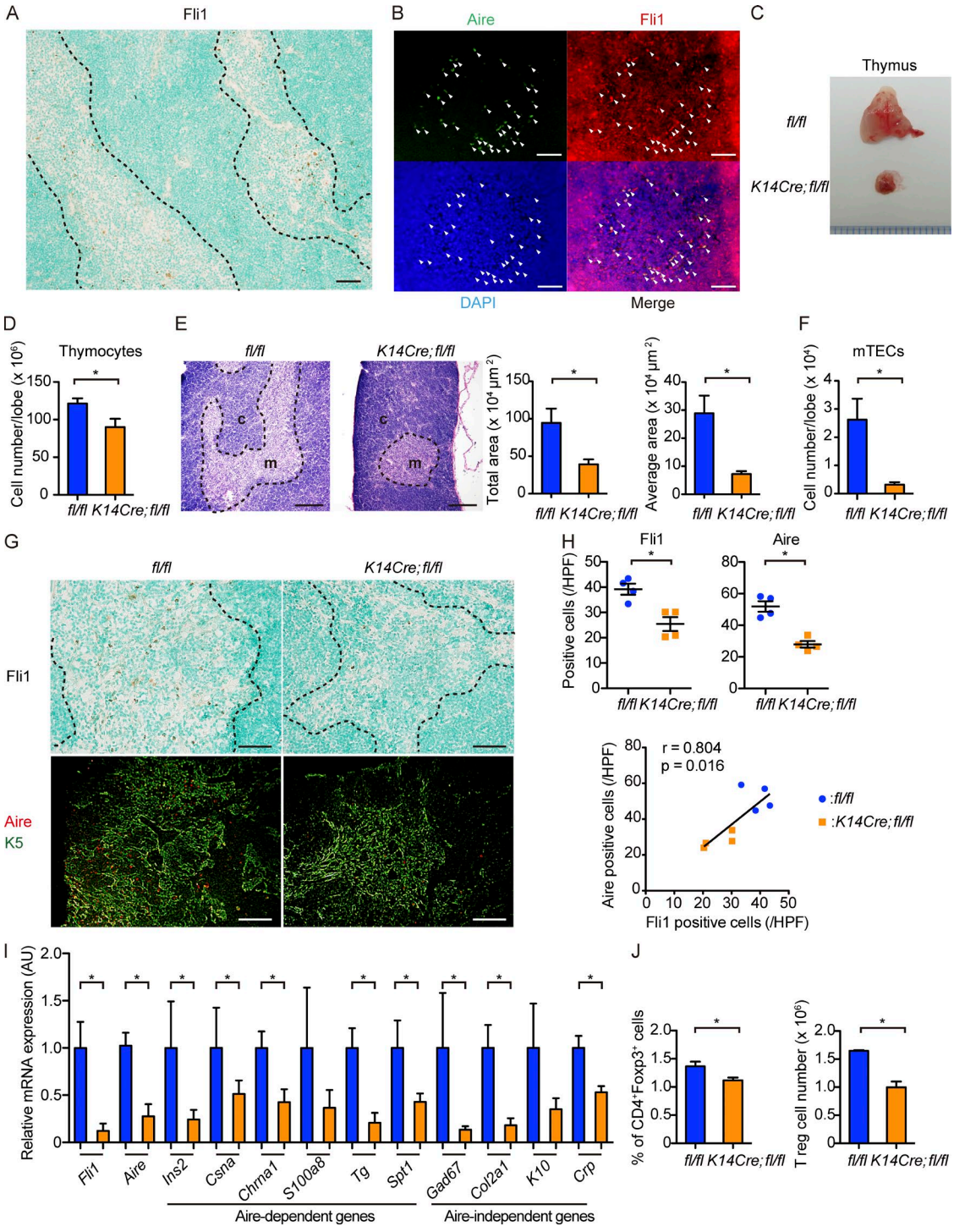

Figure 6. **mTECs robustly express Fli1, and *K14Cre;fl/fl* mice show thymic hypotrophy with decreased Aire expression.** (A and B) Immunohistochemistry for Fli1 (A) and double immunofluorescence for Aire and Fli1 (B) were performed with thymuses of 1-mo-old wild-type (C57BL/6) mice. In immunofluorescence, Aire, Fli1, and nuclei were stained with fluorescein isothiocyanate (green), Alexa Flour 555 (red), and DAPI (blue), respectively. Arrowheads indicate Aire-positive mTECs expressing Fli1. $n = 5$ mice. Bars, 50 µm. (C) Gross appearance of thymuses from 2-mo-old *fl/fl* and *K14Cre;fl/fl* mice. (D) The number of thymocytes was counted per lobe. $n = 4$ mice per genotype. (E) H&E staining of thymuses from 2-mo-old *fl/fl* and *K14Cre;fl/fl* mice. c, cortex; m, medulla. (Right) The total area of the medulla and the mean area per islet in each group. $n = 4$ per each group of mice. Bars, 200 µm. (F) Thymuses from 2-mo-old mice were subjected to flow cytometric analysis. The number of mTECs, defined as $CD45^{-}EpCAM^{+}Ly51^{-}$ cells, was calculated per lobe. $n = 4$ per group of mice. (G) Immunohistochemistry for Fli1 and double immunofluorescence for Aire and K5 with thymuses from 8-wk-old mice. K5-positive areas

and subsequent fibrosis in these organs. Thus, the down-regulation of single transcription factor Fli1 provides a useful clue to solve these two unanswered fundamental questions in SSc pathogenesis, further supporting the notion that Fli1 deficiency serves as a predisposing factor of SSc by integrating the induction of SSc-related gene programs in various types of cells (Asano, 2015).

We demonstrate that *K14Cre;fl/fl* mice develop spontaneous organ fibrosis in the skin and esophagus. The skin change of *K14Cre;fl/fl* mice reproduced SSc-like phenotype with the increased dermal thickness and the impaired collagen fibril structure together with SSc-like alterations of fibrosis- and fibrillogenesis-related gene programs (Perlish et al., 1988). Furthermore, the expression profiles of cytokines and chemokines and the pattern of inflammatory cell infiltration were quite similar between *K14Cre;fl/fl* mice and human SSc. In addition, the esophagus of *K14Cre;fl/fl* mice recapitulated the histological features of SSc esophagus, such as increased collagen content and thicker subepithelial lamina propria, as well as the gene expression profiles of cytokines and growth factors. Importantly, the induction of SSc-like phenotype was confirmed in keratinocytes and esophageal stratified squamous epithelia by immunostaining and/or quantitative RT-PCR (qRT-PCR). Indeed, there certainly exist some differences between dermal fibrosis in *K14Cre;fl/fl* mice and human SSc. For example, *K14Cre;fl/fl* mice did not exhibit adipose tissue loss, which is an important feature of skin fibrosis in SSc and its mouse models (Marangoni et al., 2015). Furthermore, alteration of collagen fibril ultrastructure was milder than in the skin of human SSc and its mouse models (Noda et al., 2014). However, the similarity of the histological and molecular features of the skin and esophagus of *K14Cre;fl/fl* mice and human SSc strongly suggests that Fli1 deficiency–dependent activation of epithelial cells contributes to fibrosis development in these two most frequently affected organs in this disease (Gabrielli et al., 2009).

Similar to human SSc, *K14Cre;fl/fl* mice spontaneously developed ILD characterized by Th2/Th17 cytokine predominance, suggesting the common pathological background between them. Because K14 is not expressed in the lungs of *K14Cre;fl/fl* mice (unpublished data), lung epithelial cells are not directly subjected to *Fli1* deletion by the Cre-LoxP system. Therefore, ILD likely results from the autoimmune reaction in these mice, as represented by the presence of autoantibodies against lung antigens. Because ILD is frequently caused by the impairment of central tolerance caused by defective thymus and/or *Aire* loss in mice (Shum et al., 2009), we hypothesized that epithelial Fli1 deficiency impairs thymic development and/or Aire expression in mTECs. Supporting this hypothesis, *K14Cre;fl/fl* mice had defective thymuses with mTECs expressing Aire at lower levels and autoreactive T cells selectively targeting the lungs. Importantly, we demonstrated that Fli1 functions as a potent transcriptional activator of the *AIRE* gene in epithelial cells. Accordingly, we concluded that epithelial Fli1 deficiency–dependent thymic defects with Aire suppression in mTECs largely contributes to ILD development in *K14Cre;fl/fl* mice and raise the possibility that such a mechanism also plays a role in SSc-ILD.

The contribution of Aire deficiency to autoimmunity has been reported in human diseases and animal models. In humans, *AIRE* gene mutations cause autoimmune polyendocrinopathy-candidiasis-ectodermal dystrophy, a primary immunodeficiency disease characterized by various autoimmune manifestations, including ILD, via disrupted central tolerance (Mathis and Benoist, 2009). Importantly, certain *AIRE* gene polymorphisms are related to SSc concomitant with autoimmune thyroiditis (Ferrera et al., 2007). In mice, defective mTEC development as observed in *Aire*-mutated mice leads to significant autoimmune phenotypes, including ILD (Akiyama et al., 2005; Shum et al., 2009). This phenotype of *Aire*-mutated mice prompted us to investigate the *Aire* gene in *K14Cre;fl/fl* mice. However, infiltrating cells in ILD of the *Aire*-mutated mice are mainly composed of Th1/Th17 cell–polarized $CD4^+$ T cells (Shum et al., 2009), thus suggesting that ILD of *Aire*-mutated mice is molecularly different from ILD in *K14Cre;fl/fl* mice and SSc. Importantly, mice with homozygous deletion of *Ets1*, a transcriptional activator of the *AIRE* gene (Murumägi et al., 2006) belonging to the same transcription family as Fli1, develop T cell–mediated systemic autoimmunity with Th2 cell–skewed polarization (Mouly et al., 2010), suggesting that the immune balance of autoreactive $CD4^+$ T cells is influenced by additional factors other than Aire in $Ets^{-/-}$ mice. In the present study, *K14Cre;fl/fl* mice demonstrated ILD with Th2/Th17 cell–skewed polarization, indicating that the combination of Aire loss together with, not yet defined, additional epithelial Fli1 deficiency–dependent factors may promote Th2/Th17 immune responses. Indeed, considering that *K14Cre;fl/fl* mice generally exhibited thymic atrophy, which is relatively rare in *Aire*-knockout mice (Ramsey et al., 2002), and ex-

indicate the thymic medulla. Bars, 50 µm. (H, top) Fli1- and Aire-positive cells per HPF were counted. (Bottom) The correlation between the numbers of Aire- and Fli1-positive cells was assessed by Spearman's correlation analysis. The solid line represents the regression line. $n = 4$ per group. (I) mRNA expression analysis for *Fli1*, *Aire*, and representative Aire-dependent and Aire-independent genes in the sorted mTECs defined as $CD45^-EpCAM^+Ly51^-$ cells. $n = 4$ per group. AU, arbitrary units. (J) Analysis on thymic T reg cells. Gates were set serially on singlets, and $CD3^+$ and $CD4^+Foxp3^+$ cells were analyzed. The proportion of $CD4^+Foxp3^+$ cells in $CD3^+$ cells (left) and the number of these cells (right) are shown. $n = 4$ mice per group. (A, E, and G) Dashed lines indicate the border between medulla and cortex. For immunofluorescence, immunohistochemistry, and H&E staining, representative images of five independent experiments are shown. Results of other experiments are from representative experiments that have been repeated three times in different pairs of mice yielding similar results. Data are shown as mean ± SEM. *, $P < 0.05$ by two-tailed Mann-Whitney *U* test.

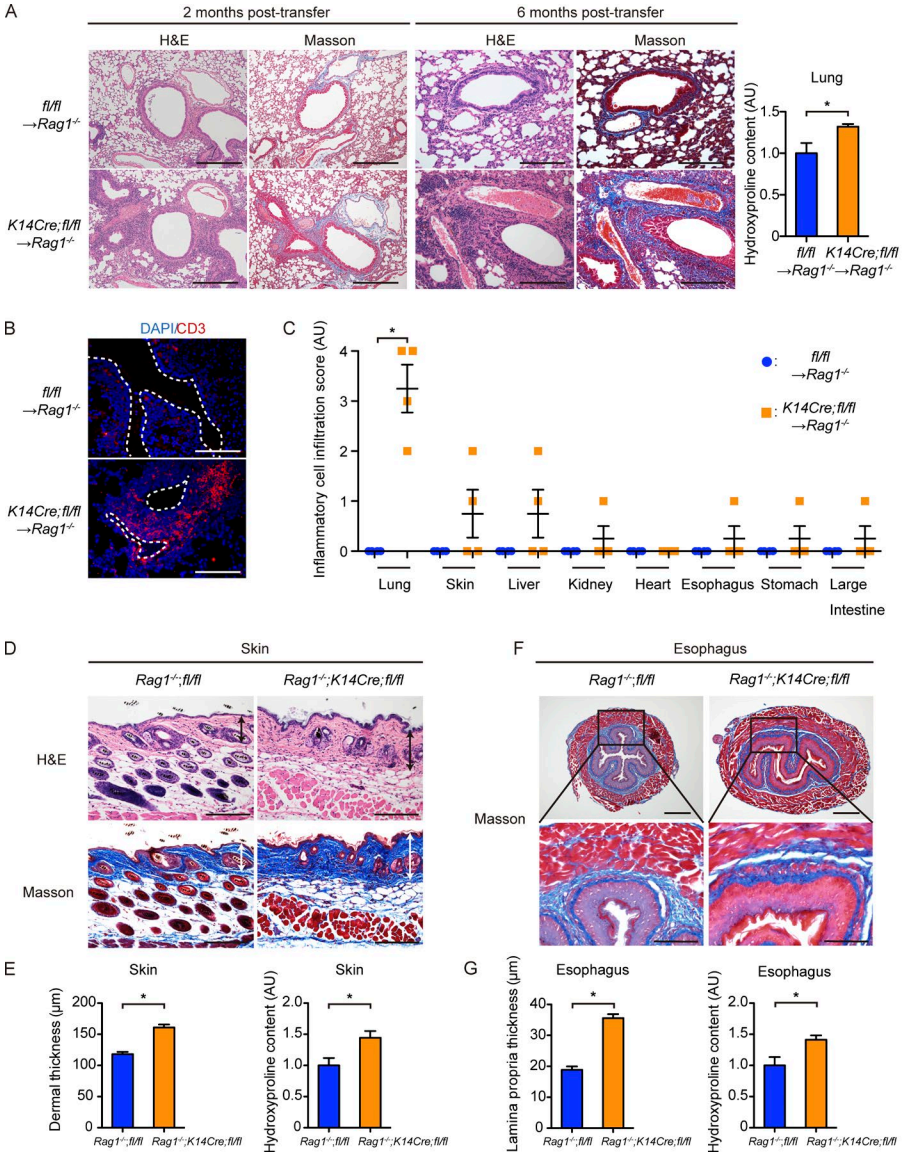

Figure 7. **Development of ILD in *K14Cre;fl/fl* mice is dependent on their autoreactive T cells, whereas skin and esophageal fibrosis is not.** (A) Representative H&E and Masson-Trichrome staining of the lungs of recipient *Rag1*$^{-/-}$ mice to which 10^6 NK1.1$^-$CD3$^+$ T cells from *fl/fl* mice or *K14Cre;fl/fl* mice were transferred 2 (left) and 6 (right) mo before. Bars, 200 µm. (Right) Collagen contents of the total left lung from the recipient mice (2 mo after transfer) were measured by hydroxyproline assay. n = 4–7 mice per group. (B) Immunofluorescence with anti-CD3 antibody and DAPI was performed using the lungs of mice under the same conditions (2 mo after transfer). White, dashed lines indicate the bronchi. Bar, 200 µm. (C) Histological evaluation of inflammatory cell infiltration to various internal organs of recipient *Rag1*$^{-/-}$ mice 6 mo after transfer. (D) H&E and Masson-Trichrome staining of the back skin of 3-mo-old *Rag1*$^{-/-}$*;K14Cre;fl/fl* and *Rag1*$^{-/-}$*;fl/fl* mice. Double-headed arrows represent dermal thickness. Bars, 200 µm. (E, left) Dermal thickness was evaluated at the age of 3 mo in each group of mice. (Right) Hydroxyproline contents of the back skin were compared between these two groups of mice. (F, top) Masson-Trichrome staining of the lower esophagus of 3-mo-old *Rag1*$^{-/-}$*;K14Cre;fl/fl* and *Rag1*$^{-/-}$*;fl/fl* mice. Bars, 500 µm. (Bottom) Higher magnification images of the regions indicated by squares in the top panels. Bars, 200 µm. (G, left) Lamina propria thickness was evaluated at the age of 3 mo in each group of mice. (Right) Hydroxyproline contents of the lower esophagus were compared between these two groups of mice. n = 4 mice per group, unless otherwise indicated. Data in graphs are shown as mean ± SEM. *, $P < 0.05$ by two-tailed Mann-Whitney U test. For histological analyses, representative images of three independent experiments are shown. Results of other experiments are from representative experiments that have been repeated twice in different pairs of mice yielding similar results. AU, arbitrary units.

tensively suppressed expression of both Aire-dependent and Aire-independent genes in mTECs, Fli1 down-regulation likely suppresses some molecules regulating TSA expression, such as transcription factor Fezf2 (Takaba et al., 2015), in addition to Aire while at the same time having additional negative effects on thymic epithelial development. Similar to this, an adaptor protein Sin regulates thymic development, and its knockdown causes defective thymic development with decreased number of mTECs as well as suppressed expression of Aire, Aire-dependent genes, and Aire-independent genes, leading to autoimmune phenotype (Danzl et al., 2010). Taking these current and previous findings together, Fli1 may affect the expression of other factors as well as Aire in mTECs. Further studies are required to clarify this point.

This study identified dysregulated epithelia as a principal driver of dermal and esophageal fibrosis in *K14Cre;fl/fl* mice through the following findings: (a) T cell transfer from *K14Cre;fl/fl* mice to *Rag1*$^{-/-}$ mice failed to reproduce dermal and esophageal fibrosis and (b) *Rag1*$^{-/-}$*;K14Cre;fl/fl* mice manifested dermal and esophageal fibrosis. At this moment, we can propose a couple of possible mechanisms explaining the association of dysregulated epithelia with tissue fibrosis. First, the straightforward explanation is that several humoral factors such as IL-1α and CTGF overproduced by

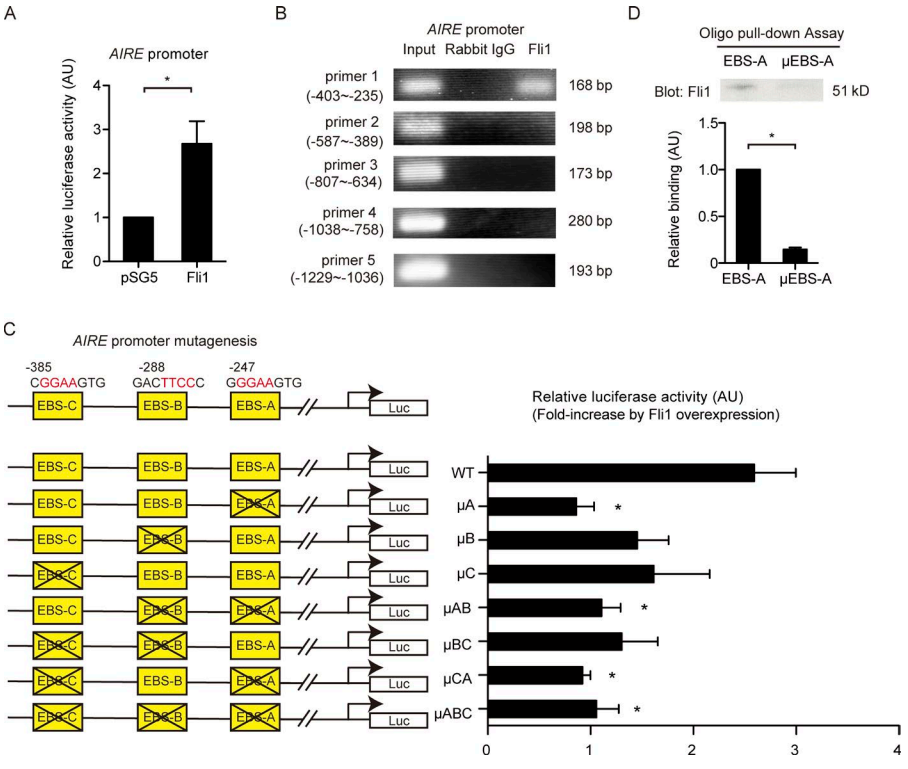

Figure 8. **Fli1 directly regulates transcription of the *AIRE* gene.** (A) Luciferase activities were measured in NHKs transfected with the *AIRE* promoter luciferase construct and either Fli1 expression vector or empty vector (pSG5). $n = 4$ per group. (B) ChIP in NHKs was performed with anti-Fli1 antibody and the primers specific for the designated areas of the *AIRE* gene promoter, covering all the EBSs between −1235 and 1. (C) Three putative Fli1 binding sites were mutated as shown in the illustration. Luciferase (Luc) activities were measured in NHKs transfected with wild-type or mutated promoter constructs together with Fli1 expression vector. Fli1-dependent induction of luciferase activities, which is normalized to luciferase activities induced by pSG5 transfection, is shown for each construct. $n = 4$ per group. The differences were compared with the results of the wild-type promoter construct. (D) The oligonucleotide pull-down assay was conducted using oligonucleotides with wild-type EBS-A or mutated EBS-A (μEBS-A). (Top) A representative blot of three independent experiments. (Bottom) The band density of each blot was measured by densitometry and summarized in the graph. In all the graphs, data are shown as mean ± SEM. *, $P < 0.05$ by two-tailed unpaired Student's *t* test. The results are from representative experiments that have been repeated twice independently, unless otherwise indicated. AU, arbitrary units.

activated epithelia directly stimulate collagen production by fibroblasts. Second, dysregulated epithelia activate innate immune cells such as macrophages and mast cells, which are present in *Rag1*$^{-/-}$ mice, resulting in fibrosis development. Indeed, there was a significantly increased number of macrophages and mast cells in parallel with fibrosis development in the skin of *K14Cre;fl/fl* mice, and up-regulated inflammatory cell infiltration was also observed in *Rag1*$^{-/-}$*;K14Cre;fl/fl* mice. Lastly, Fli1 down-regulation might contribute to enhanced EMT. EMT has been identified as a critical driver of tissue fibrosis as well as tumor progression (Nieto et al., 2016), and previous studies have disclosed its potential roles in tissue fibrosis of SSc (Wei et al., 2011; Nikitorowicz-Buniak et al., 2015). Notably, Fli1 is involved in EMT in many tumors, contributing to their progression (Scheiber et al., 2014). In the current study, Fli1-deficient NHKs strictly recapitulated EMT-like changes of SSc keratinocytes, namely heightened SNAI1 expression, despite the unaffected E-cadherin expression (Nikitorowicz-Buniak et al., 2015). This phenotype is unique for SSc keratinocytes because SNAI1 up-regulation normally leads to decreased E-cadherin expression in keratinocytes (Nieto et al., 2016). Even though it is still unclear whether SSc keratinocytes with EMT-like changes truly provide fibroblasts through EMT, our present data indicate that Fli1 deficiency strictly induces SSc-like phenotypes in keratinocytes. Further studies are required to assess these three possibilities, but it is intriguing that dysregulated epithelia may be involved in selective organ fibrosis in the skin and esophagus of SSc.

Another critical point in the experiments with *Rag1*$^{-/-}$*;K14Cre;fl/fl* mice is that the fold-increase of collagen deposition in *Rag1*$^{-/-}$*;K14Cre;fl/fl* mice compared with their control mice was considerably smaller than that between *K14Cre;fl/fl* mice and *fl/fl* mice. This evidence suggests the roles of lymphocyte activation in the development of robust tissue fibrosis in *K14Cre;fl/fl* mice. In sum, our findings indicate that dermal and esophageal fibrosis in *K14Cre;fl/fl* mice is primed by epithelial activation and subsequently promoted by the activation of the innate and adaptive immune systems. These mechanisms might have possible homology in the pathogenesis of fibrosis in human SSc.

K14Cre;fl/fl mice fulfill the criteria for a new animal model of SSc by reproducing the autoimmunity and selective organ fibrosis seen in human disease. Moreover, *K14Cre;fl/fl* mice demonstrate constitutive activation of B cells with SSc-like phenotypes. Similar to SSc B cells, B cells of *K14Cre;fl/fl* mice showed augmented expression of CD19, which functions as the dominant signaling component on B cells and

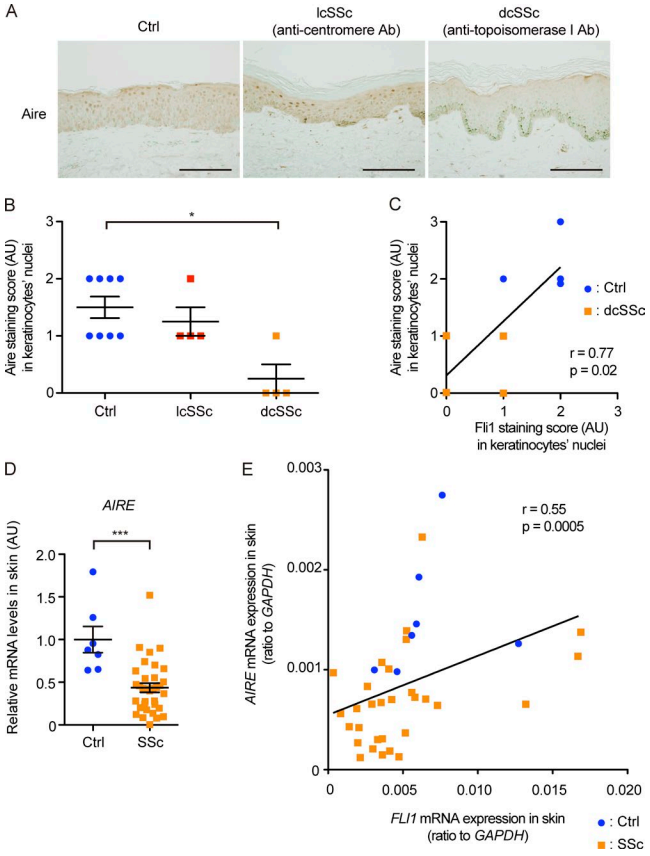

Figure 9. **Aire is expressed in the nuclei of human keratinocytes in vivo, and its expression is significantly down-regulated in SSc patients.** (A) Representative images of immunohistochemistry for Aire in healthy controls (n = 8) and lcSSc (n = 4) and dcSSc (n = 4) patients. Bars, 200 µm. (B) The signal intensities of Aire staining in the keratinocytes in A were semiquantitatively evaluated with a four-point grading scale. Kruskal-Wallis test followed by Dunn's posthoc test was used. (C) Correlation between signal intensities of Aire and Fli1 in the nuclei of keratinocytes in four dcSSc patients and four closely matched healthy controls was analyzed. (D) mRNA expression of the *AIRE* gene in skin samples from 7 healthy controls and 33 SSc patients was assessed by qRT-PCR. Two-tailed Mann-Whitney *U* test was used. (E) Correlation analysis of *AIRE* and *FLI1* mRNA expressions in the skin samples used in D (7 healthy controls and 33 SSc patients). (C and E) The solid lines indicate the regression lines. Data are shown as mean ± SEM. *, P < 0.05; ***, P < 0.0001. Ab, antibody; AU, arbitrary units; Ctrl, control.

plays a crucial role in maintaining the balance between humoral immune response and immune tolerance (Wang et al., 2012). Also, B cells of *K14Cre;fl/fl* mice produced autoantibodies and a higher amount of IgG, IgM, and IL-6. Because IL-6 enhances collagen synthesis by inducing myofibroblastic differentiation and promotes Th2/Th17 cell differentiation (Rincón et al., 1997; O'Reilly et al., 2013), its excessive production from B cells may contribute to fibrosis development in *K14Cre;fl/fl* mice. However, *K14Cre;fl/fl* mice lack the vascular abnormalities of SSc (unpublished data) recapitulated in endothelial cell–specific *Fli1* knockout mice (Asano et al., 2010b). Given the close analogy of dermal and esophageal fibrosis and autoimmunity, but not vasculopathy, between *K14Cre;fl/fl* mice and human SSc, the mechanisms driven by epithelial Fli1 deficiency might be in action in the fibrotic and immunological components of SSc.

There are several limitations to our study. First, we did not assess Fli1 protein expression in the esophagus or thymus of patients with SSc, as such specimens are largely unavailable. Therefore, we cannot exclude the possibility that dysregulation of a different set of genes causing the phenotypical alteration of epithelial cells may be contributing to SSc. Second, we did not analyze the role and significance of Aire expression in keratinocytes of human skin and its suppression in SSc. There have been only a few previous analyses on Aire expression in the skin. Among them, importantly, Clark et al. (2005) reported that human keratinocytes and fibroblasts express Aire, and co-culture system composed of these cells could induce T cell development and self-tolerance in the hematopoietic precursor cells via Aire expression in vitro. Thus, it might be possible that Fli1 deficiency leads to the decreased expression of Aire in keratinocytes, having some impacts on the peripheral immune homeostasis in the human skin. Further studies are required to clarify this point in the future.

Nonetheless, the profound similarity in autoimmunity and fibrosis between SSc and *K14Cre;fl/fl* mice seems to indicate the fundamental roles of Fli1 down-regulation in epithelial cells in SSc. In particular, our study might shed light on the fundamental yet unanswered questions in SSc research: why is SSc an autoimmune disease and why are the skin, esophagus, and lung the primary targets of fibrosis in SSc? Further investigations are awaited to elucidate the contribution of dysregulated epithelial cells to SSc development.

MATERIALS AND METHODS

Human samples

For immunohistochemical analysis of Fli1, skin samples collected from the forearm of 13 SSc patients (five patients with dcSSc with anti–topoisomerase I antibody and eight patients with lcSSc with anticentromere antibody) with skin sclerosis for <2 yr were used. For immunohistochemical analyses of Aire, skin samples collected from eight SSc patients (four patients with dcSSc with anti–topoisomerase I antibody and four patients with lcSSc with anticentromere antibody) were used. All of the patients were diagnosed with SSc based on clinical appearance and histological findings and fulfilled the new classification criteria of SSc (van den Hoogen et al., 2013). None of them had any other collagen diseases. Control specimens were obtained by skin biopsy from eight sex- and site-matched healthy donors with closely matched age. For mRNA expression analyses of the epidermis, cDNA was prepared from the epidermal sheets derived from forearm skin samples of six dcSSc patients and four healthy donors. For mRNA expression analyses of the whole skin, cDNA was prepared from the forearm skin samples of 33 SSc patients and 7 healthy donors. Institutional approval (University of

Tokyo Graduate School of Medicine) and written informed consent were obtained from all subjects. The whole study was performed according to the Declaration of Helsinki.

Mice

Fli1$^{+/-}$ and *Fli1*$^{flox/flox}$ mice were generated as described previously (Spyropoulos et al., 2000; Asano et al., 2010b). *K14Cre* (strain Tg[KRT14-cre]1Amc/J), *Rag1*$^{-/-}$, and C57BL/6 mice were purchased from The Jackson Laboratory. In the analyses of *Fli1*$^{+/-}$, *K14Cre;Fli1*$^{flox/flox}$, and *Rag1*$^{-/-}$*;K14Cre;Fli1*$^{flox/flox}$ mice, their littermate *Fli1*$^{+/+}$, *Fli1*$^{flox/flox}$, and *Rag1*$^{-/-}$*;Fli1*$^{flox/flox}$ mice were used as controls, respectively. All mice used in the experiments were female. All mice were bred in a specific pathogen–free facility. All studies and procedures were approved by the Committee on Animal Experimentation of the University of Tokyo Graduate School of Medicine.

Gene silencing of Fli1 by siRNA

NHKs (Kurabo) were transfected with 10 nM *Fli1* siRNA (Santa Cruz Biotechnology, Inc.) or control scrambled RNA (SCR; Santa Cruz Biotechnology, Inc.) for 6 h using Lipofectamine 2000 (Thermo Fisher Scientific). Thereafter, cells were cultured in MCDB153 medium lacking bovine hypothalamus extract and used for further studies.

Histological assessment, immunohistochemistry, and immunofluorescence

6-µm–thick sections of skin and internal organs were stained with H&E and Masson-Trichrome staining. Dermal thickness was examined as previously described (Takahashi et al., 2015a). The measurement of the thickness of the subcutaneous adipose tissue in the skin and the thickness of the lamina propria and circular muscle layer of the esophagus was carried out with a similar method used in the measurement of dermal thickness as conducted in previous studies (Ishikawa et al., 2009; Marangoni et al., 2015). Evaluation of the total area and mean area per islet of the thymic medulla was conducted with the method described by Danzl et al. (2010). Immunohistochemistry in mouse specimens was performed using antibodies directed against Fli1 (sc-356; Santa Cruz Biotechnology, Inc.), K6 (sc-22481; Santa Cruz Biotechnology, Inc.), K16 (MA5-13730; Thermo Fisher Scientific), IL-1α (ab9724; Abcam), IL-1β (ab9722; Abcam), CTGF (sc-14939; Santa Cruz Biotechnology, Inc.), SNAI1 (AV33314; Sigma-Aldrich), α-SMA (ab5694; Abcam), CD3 (bd555273; BD), F4/80 (MCA497; Serotec), B220 (41-0452; eBioscience), and Aire (14-5934; eBioscience). Immunohistochemistry with human skin specimens was performed with antibodies against Fli1 (sc-356; Santa Cruz Biotechnology, Inc.) and Aire (ab13573; Abcam). In the cell count of positive cells in immunohistochemical staining, stained cells were counted in 10 random grids under high power fields (HPFs) by two independent researchers (T. Takahashi. and Y. Asano) with blinded manners. For the scoring of staining intensity of immunohistochemistry, the intensities were scored by two independent researchers (T. Takahashi and Y. Asano) with blinded manners with the following scoring system: none = 0, weak = 1, moderate = 2, and strong = 3. The higher score was adopted when there was a discrepancy between the researchers. The severity of the tissue inflammation in the skin and internal organs in the recipient mice of transfer experiments was evaluated according to the scoring system by Shum et al. (2009). For immunofluorescence staining of thymuses, rat anti-Aire antibody (14-5934; eBioscience), rabbit anti-Fli1 antibody (sc-356; Santa Cruz Biotechnology, Inc.), and rabbit anti-K5 antibody (ab24647; Abcam) were used as primary antibodies. In Aire and Fli1 double staining, FITC-conjugated goat anti–rat IgG antibody (sc-2011; Santa Cruz Biotechnology, Inc.) and Alexa Fluor 555 donkey anti–rabbit IgG antibody (A31572; Thermo Fisher Scientific) and, in K5 and Aire double staining, FITC-conjugated donkey anti–rabbit IgG antibody (sc-2090; Santa Cruz Biotechnology, Inc.) and Alexa Fluor 555 goat anti–rat IgG antibody (ab150158; Abcam) were used as secondary antibodies. For immunofluorescence staining of lungs from *Rag1*$^{-/-}$ mice, rat anti-CD3 antibody (bd555273; BD) and Alexa Fluor 555 goat anti–rat IgG antibody (ab150158; Abcam) were used. Coverslips were mounted using Vectashield with DAPI (Vector Laboratories), and staining was examined with a fluorescence microscope (Bio Zero BZ-8000; Keyence) at 495 (green), 565 (red), and 400 (blue) nm. Photomicrographs of H&E staining, Masson-Trichrome staining, toluidine blue staining, and other immunohistochemical stainings were obtained with an Olympus microscope (BX51) and Olympus camera (DP73).

Collagen content measurement

Following the instructions of QuickZyme Total Collagen Assay (QuickZyme Biosciences), tissues were hydrolyzed with 6N HCl, and hydroxyproline content was quantified. 6-mm punch biopsy skin samples and total left lungs were used for the measurement of skin and lung tissue. The esophagus was marked at 2 and 5 mm from the gastroesophageal junction and cut out, and the 3-mm–length specimens were subject to the assay.

Transmission electron microscopy

Samples were collected from the back skin of 3-mo-old mice of each strain, fixed, postfixed, rinsed, dehydrated, transferred to propylene oxide, and embedded in epoxy resin. Ultrathin sections were stained with tannate, uranyl acetate, and lead citrate and examined with a microscope (JEM-1200EX; JEOL Ltd.). Multiple micrographs of cross sections of dermal collagen fibrils were chosen randomly and used for morphometry.

RNA isolation and qRT-PCR

RNA was isolated, and qRT-PCR was performed as described previously (Takahashi et al., 2015a). In the analyses for mRNA expression in the human epidermal sheets, the biopsy skin specimens were incubated in medium containing 2 U/ml Dispase II (Roche) overnight. Then, the epidermal sheets were peeled off with forceps and used for RNA isolation. In the analyses for mice epidermal sheets, ears of 3-mo-old mice were ob-

tained. The skin was mechanically detached from the cartilage and floated on the medium containing 2 U/ml Dispase II overnight. The epidermal sheet was peeled off with forceps and used for analyses as well. The sequences of the primers used are summarized in Table 1. The relative change in the levels of genes was determined by the $2^{-\Delta\Delta CT}$ method.

Measurement of immunoglobulins, IL-6, and ANA levels in the sera and/or culture supernatant

Sera from 3- and 8-mo-old mice were analyzed with ELI SA kits for the measurement of total IgG, IgM, and IgA (88-50400, 88-50470, and 88-50450; all from eBioscience). For IL-6 measurement, we used a high-sensitivity ELISA kit for

Table 1. **Primer sequences**

Species	Gene	Forward	Reverse
Human	*FLI1*	GGATGGCAAGGAACTGTGTAA	GGTTGTATAGGCCAGCAG
	AIRE	GAGAGTGCTGAGAAGGACA	GTTTAATTTCCAGGCACATGA
	IL1A	ATCAGTACCTCACGGCTGCT	TGGGTATCTCAGGCATCTCC
	K6	CTGAATGGCGAAGGCGTT	CCACTGCCGACACCACT
	K16	GACCGGCGGAGATGTGAAC	CTGCTCGTACTGGTCACGC
	CTGF	TTGCGAAGCTGACCTGGAAGAGAA	AGCTCGGTATGTCTTCATGCTGGT
	SNAI1	ACCCCAATCGGAAGCCTAACT	GGTCGTAGGGCTGCTGGAA
	CDH1	ACAACAAGCCCGAATTCACCCA	TCACAGCTGTTGCTGTTGTGCT
	GAPDH	ACCCACTCCTCCACCTTTGA	CATACCAGGAAATGAGCTTGACAA
Mouse	*Il1a*	ATGATCTGGAAGAGACCATCC	GGCAACTCCTTCAGCAACA
	Il1b	TTGACGGACCCCAAAAGAT	GAAGCTGGATGCTCTCATCTG
	Il6	GATGGATGCTACCAAACTGGAT	CCAGGTAGCTATGGTACTCCAGA
	Il8	CTGGCCGTGGCTCTCTTG	CCTTGGCAAAACTGCACCTT
	Il13	GGATATTGCATGGCCTCTGTAAC	AACAGTTGCTTTGTGTAGCTGA
	Il17a	CTCCAGAAGGCCCTCAGACTAC	AGCTTTCCCTCCGCATTGACACAG
	Tnfa	ACCCTCACACTCAGATCATCTTC	TGGTGGTTTGCTACGACGT
	Ccl2	CATCCACGTGTTGGCTCA	GATCATCTTGCTGGTGAATGAGT
	Ifng	TCAAGTGGCATAGATGTGGAAGAA	TGGCTCTGCAGGATTTTCATG
	Ctgf	GTGCCAGAACGCACACTG	CCCCGGTTACACTCCAAA
	Tgfb1	GCAACATGTGGAACTCTACCAGAA	GACGTCAAAAGACAGCCACTCA
	Col1a1	GCCAAGAAGACATCCCTGAAG	TGTGGCAGATACAGATCAAGC
	Col1a2	GGAGGGAACGGTCCACGAT	GAGTCCGCGTATCCACAA
	Adamts2	AGTGGGCCCTGAAGAAGTG	CAGAAGGCTCGGTGTACCAT
	Lum	AGATGCTTGATCTTGGAGTAAGA	CAATGAACTTGAAAAGTTTGATG
	Dcn	TGAGCTTCAACAGCATCACC	AAGTCATTTTGCCCAACTGC
	K6	TTCTCTACTTCCCAGCCTTCTCA	GCCACGGTGGCTGGTTT
	K16	GACCTCAGCCGCATTCTGA	GCGAAGCTGAGCCAGCTGCT
	Snai1	CAACTATAGCGAGCTGCAGG	ACTTGGGGTACCAGGAGAGAGT
	Ins2	AGACCATCAGCAAGCAGGTC	CTGGTGCAGCACTGATCCAC
	Csna	TGACTGGACCCTCCATTCTC	CCTTGATTCTCTCCGCTCAG
	Chrna1	GTGCTGGGCTCTTTCATCTC	TTCTGTGCGCGTTCTCATAC
	s100a8	GGAAATCACCATGCCCTCTA	GCTGTCTTTGTGAGATGCCA
	Tg	CTGTGGTGTTCTCAGCCTCAACTCC	TTGGCCTGAGTAGCAGAGGT
	Spt1	TTGTGTTGCTTGGTGTTT	TCGACTGAATCAGAGGAATCAACT
	Gad67	CACAAACTCAGCGGCATAGA	CTGGAAGAGGTAGCCTGCAC
	Col2a1	ACTGGTAAGTGGGGCAAGAC	CCACACCAAATTCCTGTTCA
	K10	AACAGATTCGGGCTGAGACC	TTCTAGCAGGCTGCGGTAGG
	Crp	TACTCTGGTGCCTTCTGATCATGA	GGCTTCTTTGACTCTGCTTCCA
	Aire	GTACAGCCGCCTGCATAGC	CCCTTTCCGGGACTGGTTTA
	Fli1	ACTTGGCCAAATGGACGGGACTAT	CCCGTAGTCAGGACTCCCG
	Gapdh	CGTGTTCCTACCCCCAATGT	TGTCATCATACTTGGCAGGTTTCT
SNAI1 ChIP primer	Amplified Region		
	−715/−472	AGAAGCTACCCTTCGGGAGA	GCATTGACGAGGGAAACG
AIRE ChIP primer	Amplified Region		
1	−403/−235	CAGGACAGGGCCACATTC	AGGGACACTTCCCTGTGATG
2	−587/−389	TAGGGGCTCTCAGCTTGTGT	GAATGTGGCCCTGTCCTG
3	−807/−634	CTTTGCTCTTTGCGTGGTC	CCTCAGAAGCCGGCGTAG
4	−1038/−759	CACTGTCCCCACTCACGTC	CTTTAAAAGGGGCACACTCG
5	−1229/−1036	GACCTCTCGTGGTTCTCTGC	TGCCCCCAGTAAAACAAGAC

The sequences of the primers used for qRT-PCR and ChIP of *SNAI1* and *AIRE* gene promoter regions are shown. The nucleotide sequences of the primers are listed in the 5′ to 3′ direction.

the measurement of sera from 1-, 2-, and 3-mo-old mice (BMS603HS; eBioscience) and otherwise used an IL-6 ELI SA kit (M600B; R&D Systems). The titers of ANA in the sera of 8-mo-old mice were analyzed with a specific ELISA kit (MBS731183; MyBioSource).

ANA detection by indirect immunofluorescence

ANA was detected by indirect immunofluorescence using human Hep-2 cells (Medical & Biological Laboratories). Sera at a 1:20 dilution from 1-, 2-, 3-, and 8-mo-old mice were incubated on the slides, followed by detection with FITC-labeled anti–mouse IgG antibody (bd553605; BD) at a 1:100 dilution using a fluorescence microscope (Bio Zero BZ-8000) at 495 nm (green).

Immunoblotting

Whole cell lysates of NHKs were subjected to sodium dodecyl sulfate–PAGE (Thermo Fisher Scientific) and immunoblotting. Bands were detected using enhanced chemiluminescent techniques (Thermo Fisher Scientific). Antibodies used were against β-actin (A1978; Sigma-Aldrich), Fli1 (sc-356; Santa Cruz Biotechnology, Inc.), K6 and K16 (MA5-14127 and MA5-13730; Thermo Fisher Scientific), IL-1α (ab9614; Abcam), CTGF (sc-14939; Santa Cruz Biotechnology, Inc.), SNAI1 (AV33314; Sigma-Aldrich), and E-cadherin (ab15148; Abcam). In experiments with lung tissue lysates from *Rag1*$^{-/-}$ mice, the homogenized lysates were incubated with sera (1:100) from *fl/fl* and *K14Cre;fl/fl* mice, followed by horseradish-peroxidase–conjugated anti–mouse IgG secondary antibody (sc-2371; Santa Cruz Biotechnology, Inc.). The protein bands were visualized with chemiluminescence. The density of each band was quantified with ImageJ software (National Institutes of Health).

ChIP assay

The ChIP assay was performed using an EpiQuik ChIP kit (Epigentek). In brief, cells were first treated with 1% formaldehyde, and cross-linked chromatin was prepared and sonicated to a mean size of 300 bp. DNA fragments were immunoprecipitated with anti-Fli1 antibody (sc-356; Santa Cruz Biotechnology, Inc.). As a negative control, normal rabbit IgG (sc-2027; Santa Cruz Biotechnology, Inc.) was used. Input corresponds to the extracted DNA from the sample before immunoprecipitation. After reversing the cross-link, the immunoprecipitated chromatin was analyzed by agarose gel electrophoresis and qRT-PCR. Primers amplifying the specific promoter regions of the *SNAI1* and *AIRE* genes were used. The sequences of the PCR primers are summarized in Table 1.

Plasmids

A human *AIRE* gene promoter luciferase construct (−1235 to 1) cloned into the pUC18 basic vector was provided by P. Peterson (University of Tartu, Tartu, Estonia; Murumägi et al., 2003, 2006). The Fli1 expression vector pSG5-Fli1 was described previously (Shirasaki et al., 1999). Site-directed mutant plasmids were generated with a QuikChange II Site-Directed Mutagenesis kit (Agilent Technologies) following the manufacturer's instructions.

Reporter gene assay

NHKs were transfected with plasmids using Lipofectamine 2000 (Thermo Fisher Scientific). Cells were harvested after 48 h, and the activities of both firefly and *Renilla* luciferase were measured with a luminometer (AB-2200; ATTO) using a dual luciferase reporter system (Promega). Firefly luciferase activity was normalized to that of *Renilla* luciferase.

Oligonucleotide pull-down assay

The oligonucleotides containing biotin on the 5′ nucleotide of the sense strand were used. The sequences of these oligonucleotides were as follows: (a) *AIRE* EBS-A oligonucleotides 5′-GCAGCGCCTCCATCACAGGGAAGTGTCCCTGCGGGAGGCC-3′ and 5′-GGCCTCCCGCAGGGACACTTCCCTGTGATGGAGGCGCTGC-3′, which correspond to base pairs −259 to −219 of *AIRE* promoter containing EBS-A and (ii) *AIRE*-mutated EBS-A oligonucleotides 5′-GCAGCGCCTCCATCACAGTTAAGTGTCCCTGCGGGAGGCC-3′ and 5′-GGCCTCCCGCAGGGACACTTAACTGTGATGGAGGCGCTGC-3′, which have mutated EBS-A (the underlined portions of sequences are the naive and mutated EBS-A). These oligonucleotides were annealed to their respective complementary oligonucleotides at 95°C for 1 hr. Nuclear extracts prepared from NHKs were incubated with streptavidin-coupled agarose beads and 500 pmol of each double-stranded oligonucleotide for 2 h at room temperature with gentle rocking. The protein–DNA–streptavidin–agarose complex was washed four times with PBS containing protease inhibitors. The precipitates were subjected to immunoblotting using the indicated antibodies.

Flow cytometric analysis

In the intracellular cytokine staining experiments, cells isolated from inguinal lymph nodes were stimulated with 10 ng/ml PMA and 1 μg/ml ionomycin (Sigma-Aldrich) in the presence of 1 μg/ml brefeldin A (BD) for 4 h. Cells were washed and stained for CD3 and CD4 (100319 and 100515; BioLegend). Samples were treated with fixative/permeabilization buffer (BD) and then stained with anti–IL-4, anti–IL-17A, and anti–IFN-γ antibodies (504123, 517007, and 505805; all from BioLegend). In the analysis of B cells, anti-B220 and anti-CD19 antibodies were used (103205 and 115507; BioLegend). Cells were analyzed on a FAC SVerse flow cytometer (BD). The positive and negative populations of cells were determined using unreactive isotype-matched antibodies as controls for background staining. Flow data were analyzed using FlowJo software (Tree Star).

T cell transfer to *Rag1*$^{-/-}$ mice and splenocyte transfer to *Rag1*$^{-/-}$*;K14Cre;fl/fl* mice

In T cell transfer experiments, single-cell suspensions from inguinal lymph nodes and spleen were stained for NK1.1 (14-5941; eBioscience) and CD3 (bd100205; BioLegend), and NK1.1^{-}CD3^{+} cells were sorted with a FACS Aria flow cytometer (BD). Sorted cells were suspended in normal saline solution in a concentration of 5×10^6 cells/ml, and 0.2 ml of cell suspension was intravenously injected into each recipient *Rag1*$^{-/-}$ mouse. 2 or 6 mo later, recipient mice were sacrificed and used for further analyses. In splenocyte transfer experiments from *fl/fl* mice to *Rag1*$^{-/-}$*;K14Cre;fl/fl* mice, splenocytes were isolated from 3-mo-old *fl/fl* mice, and 10^7 cells were transferred to 1-mo-old *Rag1*$^{-/-}$*;K14Cre;fl/fl* mice. The recipient mice were sacrificed 3 mo after transfer and used for analyses.

Isolation of B cells, culture, and measurement of supernatant IL-6 concentration

Splenic B cells were isolated by CD19-positive selection using magnetic-activated cell-sorting beads (130-052-201; Miltenyi Biotec) as described previously (Noda et al., 2014). 10^5 isolated B cells were cultured in 0.1 ml RPMI medium. Some cells were stimulated with 10 μg/ml anti-CD40 antibody (102810; BioLegend). The supernatants were harvested after 48-h incubation and subjected to measurement of IL-6 concentration by ELISA.

Isolation of mTECs

Thymuses from 8-wk-old *fl/fl* and *K14Cre;fl/fl* mice were excised, mashed with slide glasses, and then digested in the medium containing 0.15% collagenase D (Roche) and 0.1% DNase (Sigma-Aldrich) at 37°C for 30 min. Cells were filtered, centrifuged, washed in the medium, counted, and stained with anti-CD45, anti-EpCAM, and anti-Ly51 antibodies (103115, 118207, and 108307; all from BioLegend). CD45^{-}EpCAM^{+}Ly51^{-} cells were sorted using a flow cytometer (FACS Aria; BD). The number of mTECs per lobe was calculated with the number of the total cells and the proportion in the population.

Statistical analysis

Statistical analysis was performed with two-tailed unpaired Student's *t* test for two-group comparison. For comparing two group values that did not follow Gaussian distribution, a two-tailed Mann-Whitney *U* test was used. In the comparison between more than two groups (i.e., healthy controls and dcSSc/lcSSc patients), Kruskal-Wallis test with Dunn's posthoc test was used. For correlation analysis, Spearman's correlation analysis was used. $P < 0.05$ was considered statistically significant. Within-group distributions are expressed as mean ± SEM.

ACKNOWLEDGMENTS

We thank Prof. Pärt Peterson for providing us the AIRE gene promoter construct. We also thank Dr. Kaoru Morita, Dr. Keishi Fujio, and Prof. Kazuhiko Yamamoto for the technical support in flow cytometry. In addition, we appreciate the technical assistance from Natsumi Toda, Yumi Hasegawa, and Tamami Kaga for histochemical analyses.

This work was supported by Japan Society for the Promotion of Science (JSPS) KAKENHI Grant numbers JP16H05366 (to Y. Asano) and JP25293242 (to S. Sato). This study was also supported by grants from the Japan Intractable Diseases Research Foundation, the Rohto Dermatology Prize, the Japanese Society for Investigative Dermatology Fellowship Shiseido Award, the Mochida Memorial Foundation for Medical and Pharmaceutical Research, and from the Takeda Science Foundation to Y. Asano. M. Trojanowska was supported by the National Institutes of Health (grant AR042334).

The authors declare no competing financial interests.

Author contributions: T. Takahashi contributed to data collection, analysis, and manuscript writing for all experiments. Y. Asano contributed to experimental design, data analysis, and manuscript writing for all experiments. K. Nakamura, T. Yamashita, R. Saigusa, Y. Ichimura, T. Toyama, T. Taniguchi, K. Akamata, S. Noda, and A. Yoshizaki contributed to sample collection from human subjects and data analysis for all experiments. K. Sugawara and D. Tsuruta contributed to electron microscopic analysis. M. Trojanowska produced plasmids and contributed to manuscript writing. S. Sato contributed to experimental design, data analysis, and manuscript writing for all experiments.

Submitted: 18 February 2016
Revised: 8 November 2016
Accepted: 17 January 2017

REFERENCES

Aden, N., A. Nuttall, X. Shiwen, P. de Winter, A. Leask, C.M. Black, C.P. Denton, D.J. Abraham, and R.J. Stratton. 2010. Epithelial cells promote fibroblast activation via IL-1α in systemic sclerosis. *J. Invest. Dermatol.* 130:2191–2200. http://dx.doi.org/10.1038/jid.2010.120

Agarwal, S.K., and J.D. Reveille. 2010. The genetics of scleroderma (systemic sclerosis). *Curr. Opin. Rheumatol.* 22:133–138. http://dx.doi.org/10.1097/BOR.0b013e3283367c17

Akamata, K., Y. Asano, T. Taniguchi, T. Yamashita, R. Saigusa, K. Nakamura, S. Noda, N. Aozasa, T. Toyama, T. Takahashi, et al. 2015a. Increased expression of chemerin in endothelial cells due to Fli1 deficiency may contribute to the development of digital ulcers in systemic sclerosis. *Rheumatology (Oxford).* 54:1308–1316. http://dx.doi.org/10.1093/rheumatology/keu479

Akamata, K., Y. Asano, T. Yamashita, S. Noda, T. Taniguchi, T. Takahashi, Y. Ichimura, T. Toyama, M. Trojanowska, and S. Sato. 2015b. Endothelin receptor blockade ameliorates vascular fragility in endothelial cell-specific Fli-1–knockout mice by increasing Fli-1 DNA binding ability. *Arthritis Rheumatol.* 67:1335–1344. http://dx.doi.org/10.1002/art.39062

Akiyama, T., S. Maeda, S. Yamane, K. Ogino, M. Kasai, F. Kajiura, M. Matsumoto, and J. Inoue. 2005. Dependence of self-tolerance on TRAF6-directed development of thymic stroma. *Science.* 308:248–251. http://dx.doi.org/10.1126/science.1105677

Anderson, M.S., E.S. Venanzi, L. Klein, Z. Chen, S.P. Berzins, S.J. Turley, H. von Boehmer, R. Bronson, A. Dierich, C. Benoist, and D. Mathis. 2002. Projection of an immunological self shadow within the thymus by the Aire protein. *Science.* 298:1395–1401. http://dx.doi.org/10.1126/science.1075958

Asano, Y. 2010. Future treatments in systemic sclerosis. *J. Dermatol.* 37:54–70. http://dx.doi.org/10.1111/j.1346-8138.2009.00758.x

Asano, Y. 2015. Epigenetic suppression of Fli1, a potential predisposing factor in the pathogenesis of systemic sclerosis. *Int. J. Biochem. Cell Biol.* 67:86–91. http://dx.doi.org/10.1016/j.biocel.2015.06.004

Asano, Y., and S. Sato. 2015. Vasculopathy in scleroderma. *Semin. Immunopathol.* 37:489–500. http://dx.doi.org/10.1007/s00281-015-0505-5

Asano, Y., M. Markiewicz, M. Kubo, G. Szalai, D.K. Watson, and M. Trojanowska. 2009. Transcription factor Fli1 regulates collagen

fibrillogenesis in mouse skin. *Mol. Cell. Biol.* 29:425–434. http://dx.doi.org/10.1128/MCB.01278-08

Asano, Y., A.M. Bujor, and M. Trojanowska. 2010a. The impact of Fli1 deficiency on the pathogenesis of systemic sclerosis. *J. Dermatol. Sci.* 59:153–162. http://dx.doi.org/10.1016/j.jdermsci.2010.06.008

Asano, Y., L. Stawski, F. Hant, K. Highland, R. Silver, G. Szalai, D.K. Watson, and M. Trojanowska. 2010b. Endothelial Fli1 deficiency impairs vascular homeostasis: a role in scleroderma vasculopathy. *Am. J. Pathol.* 176:1983–1998. http://dx.doi.org/10.2353/ajpath.2010.090593

Assassi, S., W.R. Swindell, M. Wu, F.D. Tan, D. Khanna, D.E. Furst, D.P. Tashkin, R.R. Jahan-Tigh, M.D. Mayes, J.E. Gudjonsson, and J.T. Chang. 2015. Dissecting the heterogeneity of skin gene expression patterns in systemic sclerosis. *Arthritis Rheumatol.* 67:3016–3026. http://dx.doi.org/10.1002/art.39289

Boin, F., and A. Rosen. 2007. Autoimmunity in systemic sclerosis: current concepts. *Curr. Rheumatol. Rep.* 9:165–172. http://dx.doi.org/10.1007/s11926-007-0012-3

Clark, R.A., K. Yamanaka, M. Bai, R. Dowgiert, and T.S. Kupper. 2005. Human skin cells support thymus-independent T cell development. *J. Clin. Invest.* 115:3239–3249. http://dx.doi.org/10.1172/JCI24731

Danzl, N.M., L.T. Donlin, and K. Alexandropoulos. 2010. Regulation of medullary thymic epithelial cell differentiation and function by the signaling protein Sin. *J. Exp. Med.* 207:999–1013. http://dx.doi.org/10.1084/jem.20092384

Ferrera, F., M. Rizzi, B. Sprecacenere, P. Balestra, M. Sessarego, A. Di Carlo, G. Filaci, A. Gabrielli, R. Ravazzolo, and F. Indiveri. 2007. *AIRE* gene polymorphisms in systemic sclerosis associated with autoimmune thyroiditis. *Clin. Immunol.* 122:13–17. http://dx.doi.org/10.1016/j.clim.2006.09.013

Fleischmajer, R., J.S. Perlish, and J.R. Reeves. 1977. Cellular infiltrates in scleroderma skin. *Arthritis Rheum.* 20:975–984. http://dx.doi.org/10.1002/art.1780200410

Gabrielli, A., E.V. Avvedimento, and T. Krieg. 2009. Scleroderma. *N. Engl. J. Med.* 360:1989–2003. http://dx.doi.org/10.1056/NEJMra0806188

Hamaguchi, Y. 2010. Autoantibody profiles in systemic sclerosis: predictive value for clinical evaluation and prognosis. *J. Dermatol.* 37:42–53. http://dx.doi.org/10.1111/j.1346-8138.2009.00762.x

Harris, M.L., and A. Rosen. 2003. Autoimmunity in scleroderma: the origin, pathogenetic role, and clinical significance of autoantibodies. *Curr. Opin. Rheumatol.* 15:778–784. http://dx.doi.org/10.1097/00002281-200311000-00016

Hobbs, R.P., D.J. DePianto, J.T. Jacob, M.C. Han, B.M. Chung, A.S. Batazzi, B.G. Poll, Y. Guo, J. Han, S. Ong, et al. 2015. Keratin-dependent regulation of Aire and gene expression in skin tumor keratinocytes. *Nat. Genet.* 47:933–938. http://dx.doi.org/10.1038/ng.3355

Ichimura, Y., Y. Asano, K. Akamata, S. Noda, T. Taniguchi, T. Takahashi, T. Toyama, Y. Tada, M. Sugaya, S. Sato, and T. Kadono. 2015. Progranulin overproduction due to Fli-1 deficiency contributes to the resistance of dermal fibroblasts to tumor necrosis factor in systemic sclerosis. *Arthritis Rheumatol.* 67:3245–3255. http://dx.doi.org/10.1002/art.39312

Ishikawa, H., K. Takeda, A. Okamoto, S. Matsuo, and K. Isobe. 2009. Induction of autoimmunity in a bleomycin-induced murine model of experimental systemic sclerosis: an important role for $CD4^+$ T cells. *J. Invest. Dermatol.* 129:1688–1695. http://dx.doi.org/10.1038/jid.2008.431

Jordan, S., J.H.W. Distler, B. Maurer, D. Huscher, J.M. van Laar, Y. Allanore, and O. Distler. EUSTAR Rituximab study group. 2015. Effects and safety of rituximab in systemic sclerosis: an analysis from the European Scleroderma Trial and Research (EUSTAR) group. *Ann. Rheum. Dis.* 74:1188–1194. http://dx.doi.org/10.1136/annrheumdis-2013-204522

Joseph, C.G., E. Darrah, A.A. Shah, A.D. Skora, L.A. Casciola-Rosen, F.M. Wigley, F. Boin, A. Fava, C. Thoburn, I. Kinde, et al. 2014. Association of the autoimmune disease scleroderma with an immunologic response to cancer. *Science.* 343:152–157. http://dx.doi.org/10.1126/science.1246886

Kawaguchi, Y., S.A. McCarthy, S.C. Watkins, and T.M. Wright. 2004. Autocrine activation by interleukin 1alpha induces the fibrogenic phenotype of systemic sclerosis fibroblasts. *J. Rheumatol.* 31:1946–1954.

Khan, K., S. Xu, S. Nihtyanova, E. Derrett-Smith, D. Abraham, C.P. Denton, and V.H. Ong. 2012. Clinical and pathological significance of interleukin 6 overexpression in systemic sclerosis. *Ann. Rheum. Dis.* 71:1235–1242. http://dx.doi.org/10.1136/annrheumdis-2011-200955

Kont, V., M. Laan, K. Kisand, A. Merits, H.S. Scott, and P. Peterson. 2008. Modulation of Aire regulates the expression of tissue-restricted antigens. *Mol. Immunol.* 45:25–33. http://dx.doi.org/10.1016/j.molimm.2007.05.014

Kubo, M., J. Czuwara-Ladykowska, O. Moussa, M. Markiewicz, E. Smith, R.M. Silver, S. Jablonska, M. Blaszczyk, D.K. Watson, and M. Trojanowska. 2003. Persistent down-regulation of Fli1, a suppressor of collagen transcription, in fibrotic scleroderma skin. *Am. J. Pathol.* 163:571–581. http://dx.doi.org/10.1016/S0002-9440(10)63685-1

Kumar, V., L.A. Pedroza, E.M. Mace, S. Seeholzer, G. Cotsarelis, A. Condino-Neto, A.S. Payne, and J.S. Orange. 2011. The autoimmune regulator (AIRE), which is defective in autoimmune polyendocrinopathy-candidiasis-ectodermal dystrophy patients, is expressed in human epidermal and follicular keratinocytes and associates with the intermediate filament protein cytokeratin 17. *Am. J. Pathol.* 178:983–988. http://dx.doi.org/10.1016/j.ajpath.2010.12.007

Lafyatis, R., C. O'Hara, C.A. Feghali-Bostwick, and E. Matteson. 2007. B cell infiltration in systemic sclerosis-associated interstitial lung disease. *Arthritis Rheum.* 56:3167–3168. http://dx.doi.org/10.1002/art.22847

Lafyatis, R., E. Kissin, M. York, G. Farina, K. Viger, M.J. Fritzler, P.A. Merkel, and R.W. Simms. 2009. B cell depletion with rituximab in patients with diffuse cutaneous systemic sclerosis. *Arthritis Rheum.* 60:578–583. http://dx.doi.org/10.1002/art.24249

Leask, A. 2009. Signaling in fibrosis: targeting the TGF beta, endothelin-1 and CCN2 axis in scleroderma. *Front. Biosci. (Elite Ed.).* 1:115–122.

LeRoy, E.C., C. Black, R. Fleischmajer, S. Jablonska, T. Krieg, T.A. Medsger Jr., N. Rowell, and F. Wollheim. 1988. Scleroderma (systemic sclerosis): classification, subsets and pathogenesis. *J. Rheumatol.* 15:202–205.

Liston, A., D.H. Gray, S. Lesage, A.L. Fletcher, J. Wilson, K.E. Webster, H.S. Scott, R.L. Boyd, L. Peltonen, and C.C. Goodnow. 2004. Gene dosage–limiting role of *Aire* in thymic expression, clonal deletion, and organ-specific autoimmunity. *J. Exp. Med.* 200:1015–1026. http://dx.doi.org/10.1084/jem.20040581

Manetti, M., E. Neumann, A.F. Milia, I.H. Tarner, P. Bechi, M. Matucci-Cerinic, L. Ibba-Manneschi, and U. Müller-Ladner. 2007. Severe fibrosis and increased expression of fibrogenic cytokines in the gastric wall of systemic sclerosis patients. *Arthritis Rheum.* 56:3442–3447. http://dx.doi.org/10.1002/art.22940

Marangoni, R.G., B.D. Korman, J. Wei, T.A. Wood, L.V. Graham, M.L. Whitfield, P.E. Scherer, W.G. Tourtellotte, and J. Varga. 2015. Myofibroblasts in murine cutaneous fibrosis originate from adiponectin-positive intradermal progenitors. *Arthritis Rheumatol.* 67:1062–1073. http://dx.doi.org/10.1002/art.38990

Mathis, D., and C. Benoist. 2009. Aire. *Annu. Rev. Immunol.* 27:287–312. http://dx.doi.org/10.1146/annurev.immunol.25.022106.141532

Matsumoto, M. 2011. Contrasting models for the roles of Aire in the differentiation program of epithelial cells in the thymic medulla. *Eur. J. Immunol.* 41:12–17. http://dx.doi.org/10.1002/eji.201041024

Mélet, F., B. Motro, D.J. Rossi, L. Zhang, and A. Bernstein. 1996. Generation of a novel Fli-1 protein by gene targeting leads to a defect in thymus development and a delay in Friend virus-induced erythroleukemia. *Mol. Cell. Biol.* 16:2708–2718. http://dx.doi.org/10.1128/MCB.16.6.2708

Mouly, E., K. Chemin, H.V. Nguyen, M. Chopin, L. Mesnard, M. Leite-de-Moraes, O. Burlen-defranoux, A. Bandeira, and J.C. Bories. 2010. The Ets-1 transcription factor controls the development and function of natural regulatory T cells. *J. Exp. Med.* 207:2113–2125. http://dx.doi.org/10.1084/jem.20092153

Murumägi, A., P. Vähämurto, and P. Peterson. 2003. Characterization of regulatory elements and methylation pattern of the autoimmune regulator (AIRE) promoter. *J. Biol. Chem.* 278:19784–19790. http://dx.doi.org/10.1074/jbc.M210437200

Murumägi, A., O. Silvennoinen, and P. Peterson. 2006. Ets transcription factors regulate AIRE gene promoter. *Biochem. Biophys. Res. Commun.* 348:768–774. http://dx.doi.org/10.1016/j.bbrc.2006.07.135

Nakamura, M., and Y. Tokura. 2011. Expression of SNAI1 and TWIST1 in the eccrine glands of patients with systemic sclerosis: possible involvement of epithelial-mesenchymal transition in the pathogenesis. *Br. J. Dermatol.* 164:204–205. http://dx.doi.org/10.1111/j.1365-2133.2010.10021.x

Nieto, M.A., R.Y. Huang, R.A. Jackson, and J.P. Thiery. 2016. Emt: 2016. *Cell.* 166:21–45. http://dx.doi.org/10.1016/j.cell.2016.06.028

Nikitorowicz-Buniak, J., X. Shiwen, C.P. Denton, D. Abraham, and R. Stratton. 2014. Abnormally differentiating keratinocytes in the epidermis of systemic sclerosis patients show enhanced secretion of CCN2 and S100A9. *J. Invest. Dermatol.* 134:2693–2702. http://dx.doi.org/10.1038/jid.2014.253

Nikitorowicz-Buniak, J., C.P. Denton, D. Abraham, and R. Stratton. 2015. Partially evoked epithelial-mesenchymal transition (EMT) is associated with increased TGFβ signaling within lesional scleroderma skin. *PLoS One.* 10:e0134092. http://dx.doi.org/10.1371/journal.pone.0134092

Noda, S., Y. Asano, K. Akamata, N. Aozasa, T. Taniguchi, T. Takahashi, Y. Ichimura, T. Toyama, H. Sumida, K. Yanaba, et al. 2012. A possible contribution of altered cathepsin B expression to the development of skin sclerosis and vasculopathy in systemic sclerosis. *PLoS One.* 7:e32272. http://dx.doi.org/10.1371/journal.pone.0032272

Noda, S., Y. Asano, T. Takahashi, K. Akamata, N. Aozasa, T. Taniguchi, Y. Ichimura, T. Toyama, H. Sumida, Y. Kuwano, et al. 2013. Decreased cathepsin V expression due to Fli1 deficiency contributes to the development of dermal fibrosis and proliferative vasculopathy in systemic sclerosis. *Rheumatology (Oxford).* 52:790–799. http://dx.doi.org/10.1093/rheumatology/kes379

Noda, S., Y. Asano, S. Nishimura, T. Taniguchi, K. Fujiu, I. Manabe, K. Nakamura, T. Yamashita, R. Saigusa, K. Akamata, et al. 2014. Simultaneous downregulation of KLF5 and Fli1 is a key feature underlying systemic sclerosis. *Nat. Commun.* 5:5797. http://dx.doi.org/10.1038/ncomms6797

O'Reilly, S., T. Hügle, and J.M. van Laar. 2012. T cells in systemic sclerosis: a reappraisal. *Rheumatology (Oxford).* 51:1540–1549. http://dx.doi.org/10.1093/rheumatology/kes090

O'Reilly, S., R. Cant, M. Ciechomska, and J.M. van Laar. 2013. Interleukin-6: a new therapeutic target in systemic sclerosis? *Clin. Transl. Immunology.* 2:e4. http://dx.doi.org/10.1038/cti.2013.2

Perlish, J.S., G. Lemlich, and R. Fleischmajer. 1988. Identification of collagen fibrils in scleroderma skin. *J. Invest. Dermatol.* 90:48–54. http://dx.doi.org/10.1111/1523-1747.ep12462561

Qiu, W., X. Li, H. Tang, A.S. Huang, A.A. Panteleyev, D.M. Owens, and G.H. Su. 2011. Conditional activin receptor type 1B (Acvr1b) knockout mice reveal hair loss abnormality. *J. Invest. Dermatol.* 131:1067–1076. http://dx.doi.org/10.1038/jid.2010.400

Ramsey, C., O. Winqvist, L. Puhakka, M. Halonen, A. Moro, O. Kämpe, P. Eskelin, M. Pelto-Huikko, and L. Peltonen. 2002. Aire deficient mice develop multiple features of APECED phenotype and show altered immune response. *Hum. Mol. Genet.* 11:397–409. http://dx.doi.org/10.1093/hmg/11.4.397

Rangel-Moreno, J., L. Hartson, C. Navarro, M. Gaxiola, M. Selman, and T.D. Randall. 2006. Inducible bronchus-associated lymphoid tissue (iBALT) in patients with pulmonary complications of rheumatoid arthritis. *J. Clin. Invest.* 116:3183–3194. http://dx.doi.org/10.1172/JCI28756

Rieder, F., P. Biancani, K. Harnett, L. Yerian, and G.W. Falk. 2010. Inflammatory mediators in gastroesophageal reflux disease: impact on esophageal motility, fibrosis, and carcinogenesis. *Am. J. Physiol. Gastrointest. Liver Physiol.* 298:G571–G581. http://dx.doi.org/10.1152/ajpgi.00454.2009

Rincón, M., J. Anguita, T. Nakamura, E. Fikrig, and R.A. Flavell. 1997. Interleukin (IL)-6 directs the differentiation of IL-4–producing $CD4^+$ T cells. *J. Exp. Med.* 185:461–470. http://dx.doi.org/10.1084/jem.185.3.461

Roberts, C.G., L.K. Hummers, W.J. Ravich, F.M. Wigley, and G.M. Hutchins. 2006. A case-control study of the pathology of oesophageal disease in systemic sclerosis (scleroderma). *Gut.* 55:1697–1703. http://dx.doi.org/10.1136/gut.2005.086074

Romano, E., I. Chora, M. Manetti, C. Mazzotta, I. Rosa, S. Bellando-Randone, J. Blagojevic, R. Soares, J. Avouac, Y. Allanore, et al. 2016. Decreased expression of neuropilin-1 as a novel key factor contributing to peripheral microvasculopathy and defective angiogenesis in systemic sclerosis. *Ann. Rheum. Dis.* 75:1541–1549. http://dx.doi.org/10.1136/annrheumdis-2015-207483

Saigusa, R., Y. Asano, T. Taniguchi, T. Yamashita, T. Takahashi, Y. Ichimura, T. Toyama, Z. Tamaki, Y. Tada, M. Sugaya, et al. 2015. A possible contribution of endothelial CCN1 downregulation due to Fli1 deficiency to the development of digital ulcers in systemic sclerosis. *Exp. Dermatol.* 24:127–132. http://dx.doi.org/10.1111/exd.12602

Saito, E., M. Fujimoto, M. Hasegawa, K. Komura, Y. Hamaguchi, Y. Kaburagi, T. Nagaoka, K. Takehara, T.F. Tedder, and S. Sato. 2002. CD19-dependent B lymphocyte signaling thresholds influence skin fibrosis and autoimmunity in the tight-skin mouse. *J. Clin. Invest.* 109:1453–1462. http://dx.doi.org/10.1172/JCI0215078

Sano, S., Y. Takahama, T. Sugawara, H. Kosaka, S. Itami, K. Yoshikawa, J. Miyazaki, W. van Ewijk, and J. Takeda. 2001. Stat3 in thymic epithelial cells is essential for postnatal maintenance of thymic architecture and thymocyte survival. *Immunity.* 15:261–273. http://dx.doi.org/10.1016/S1074-7613(01)00180-7

Sato, S., M. Hasegawa, M. Fujimoto, T.F. Tedder, and K. Takehara. 2000. Quantitative genetic variation in CD19 expression correlates with autoimmunity. *J. Immunol.* 165:6635–6643. http://dx.doi.org/10.4049/jimmunol.165.11.6635

Sato, S., M. Fujimoto, M. Hasegawa, K. Takehara, and T.F. Tedder. 2004. Altered B lymphocyte function induces systemic autoimmunity in systemic sclerosis. *Mol. Immunol.* 41:1123–1133. http://dx.doi.org/10.1016/j.molimm.2004.06.025

Scheiber, M.N., P.M. Watson, T. Rumboldt, C. Stanley, R.C. Wilson, V.J. Findlay, P.E. Anderson, and D.K. Watson. 2014. FLI1 expression is correlated with breast cancer cellular growth, migration, and invasion and altered gene expression. *Neoplasia.* 16:801–813. http://dx.doi.org/10.1016/j.neo.2014.08.007

Shirasaki, F., H.A. Makhluf, C. LeRoy, D.K. Watson, and M. Trojanowska. 1999. Ets transcription factors cooperate with Sp1 to activate the human tenascin-C promoter. *Oncogene.* 18:7755–7764. http://dx.doi.org/10.1038/sj.onc.1203360

Shum, A.K., J. DeVoss, C.L. Tan, Y. Hou, K. Johannes, C.S. O'Gorman, K.D. Jones, E.B. Sochett, L. Fong, and M.S. Anderson. 2009. Identification of an autoantigen demonstrates a link between interstitial lung disease and a defect in central tolerance. *Sci. Transl. Med.* 1:9ra20. http://dx.doi.org/10.1126/scitranslmed.3000284

Spyropoulos, D.D., P.N. Pharr, K.R. Lavenburg, P. Jackers, T.S. Papas, M. Ogawa, and D.K. Watson. 2000. Hemorrhage, impaired hematopoiesis, and lethality in mouse embryos carrying a targeted disruption of the Fli1 transcription factor. *Mol. Cell. Biol.* 20:5643–5652. http://dx.doi.org/10.1128/MCB.20.15.5643-5652.2000

Sukseree, S., M. Mildner, H. Rossiter, J. Pammer, C.F. Zhang, R. Watanapokasin, E. Tschachler, and L. Eckhart. 2012. Autophagy in the thymic epithelium is dispensable for the development of self-tolerance in a novel mouse model. *PLoS One.* 7:e38933. http://dx.doi.org/10.1371/journal.pone.0038933

Suwara, M.I., N.J. Green, L.A. Borthwick, J. Mann, K.D. Mayer-Barber, L. Barron, P.A. Corris, S.N. Farrow, T.A. Wynn, A.J. Fisher, and D.A. Mann. 2014. IL-1α released from damaged epithelial cells is sufficient and essential to trigger inflammatory responses in human lung fibroblasts. *Mucosal Immunol.* 7:684–693. http://dx.doi.org/10.1038/mi.2013.87

Takaba, H., Y. Morishita, Y. Tomofuji, L. Danks, T. Nitta, N. Komatsu, T. Kodama, and H. Takayanagi. 2015. Fezf2 orchestrates a thymic program of self-antigen expression for immune tolerance. *Cell.* 163:975–987. http://dx.doi.org/10.1016/j.cell.2015.10.013

Takahashi, T., Y. Asano, Y. Ichimura, T. Toyama, T. Taniguchi, S. Noda, K. Akamata, Y. Tada, M. Sugaya, T. Kadono, and S. Sato. 2015a. Amelioration of tissue fibrosis by toll-like receptor 4 knockout in murine models of systemic sclerosis. *Arthritis Rheumatol.* 67:254–265. http://dx.doi.org/10.1002/art.38901

Takahashi, T., Y. Asano, S. Noda, N. Aozasa, K. Akamata, T. Taniguchi, Y. Ichimura, T. Toyama, H. Sumida, Y. Kuwano, et al. 2015b. A possible contribution of lipocalin-2 to the development of dermal fibrosis, pulmonary vascular involvement and renal dysfunction in systemic sclerosis. *Br. J. Dermatol.* 173:681–689. http://dx.doi.org/10.1111/bjd.13779

Taniguchi, T., Y. Asano, K. Akamata, S. Noda, T. Takahashi, Y. Ichimura, T. Toyama, M. Trojanowska, and S. Sato. 2015. Fibrosis, vascular activation, and immune abnormalities resembling systemic sclerosis in bleomycin-treated Fli-1–haploinsufficient mice. *Arthritis Rheumatol.* 67:517–526. http://dx.doi.org/10.1002/art.38948

Taroni, J.N., V. Martyanov, C.C. Huang, J.M. Mahoney, I. Hirano, B. Shetuni, G.Y. Yang, D. Brenner, B. Jung, T.A. Wood, et al. 2015. Molecular characterization of systemic sclerosis esophageal pathology identifies inflammatory and proliferative signatures. *Arthritis Res. Ther.* 17:194. http://dx.doi.org/10.1186/s13075-015-0695-1

van Bon, L., A.J. Affandi, J. Broen, R.B. Christmann, R.J. Marijnissen, L. Stawski, G.A. Farina, G. Stifano, A.L. Mathes, M. Cossu, et al. 2014. Proteome-wide analysis and CXCL4 as a biomarker in systemic sclerosis. *N. Engl. J. Med.* 370:433–443. http://dx.doi.org/10.1056/NEJMoa1114576

van den Hoogen, F., D. Khanna, J. Fransen, S.R. Johnson, M. Baron, A. Tyndall, M. Matucci-Cerinic, R.P. Naden, T.A. Medsger Jr., P.E. Carreira, et al. 2013. 2013 classification criteria for systemic sclerosis: an American College of Rheumatology/European League against Rheumatism collaborative initiative. *Arthritis Rheum.* 65:2737–2747. http://dx.doi.org/10.1002/art.38098

Wang, K., G. Wei, and D. Liu. 2012. CD19: a biomarker for B cell development, lymphoma diagnosis and therapy. *Exp. Hematol. Oncol.* 1:36. http://dx.doi.org/10.1186/2162-3619-1-36

Wang, Y., P.S. Fan, and B. Kahaleh. 2006. Association between enhanced type I collagen expression and epigenetic repression of the FLI1 gene in scleroderma fibroblasts. *Arthritis Rheum.* 54:2271–2279. http://dx.doi.org/10.1002/art.21948

Wei, J., S. Bhattacharyya, W.G. Tourtellotte, and J. Varga. 2011. Fibrosis in systemic sclerosis: emerging concepts and implications for targeted therapy. *Autoimmun. Rev.* 10:267–275. http://dx.doi.org/10.1016/j.autrev.2010.09.015

Whitfield, M.L., D.R. Finlay, J.I. Murray, O.G. Troyanskaya, J.T. Chi, A. Pergamenschikov, T.H. McCalmont, P.O. Brown, D. Botstein, and M.K. Connolly. 2003. Systemic and cell type-specific gene expression patterns in scleroderma skin. *Proc. Natl. Acad. Sci. USA.* 100:12319–12324. http://dx.doi.org/10.1073/pnas.1635114100

Wilson, M.S., and T.A. Wynn. 2009. Pulmonary fibrosis: pathogenesis, etiology and regulation. *Mucosal Immunol.* 2:103–121. http://dx.doi.org/10.1038/mi.2008.85